Modification and Utilization of Nanoporous Gold for Loading and Release of Drugs

Ibtisam Al-badri

University of Missouri–St. Louis, MO

A Dissertation Submitted to the Graduate School at the University of Missouri–St. Louis

In Partial Fulfillment of the Requirements for the Degree

Master's in Physics

December 2016

Advisory Committee

Prof. Keith J. Stine, Ph.D. (Chairperson)

Prof. Philip Fraundorf, Ph.D.

Prof. Eric Majzoub, Ph.D.

ABSTRACT

Nanoporous gold (np-Au) is a sponge-like structure of gold, which can be created by removing the less noble element from the precursor alloy, most typically silver or copper, using different chemical or electrochemical methods. It consists of interconnected ligaments and gaps between the ligaments, whose width can range from a few nanometers to a few hundreds of nanometers, creating a high surface area-to-volume ratio. Due to its many important properties (e.g., conductivity, high surface area-to-volume ratio, plasmonic response, biocompatibility, chemically inertness, and physically robustness), np-Au is suitable for different types of applications, including as a transducer for biosensors, in catalysis, for biomolecule separation, as a substrate for enzyme immobilization, and in drug delivery.

The widths of the ligaments and gaps of np-Au can be easily tuned by varying conditions during the pre- or post-production process, for example, time kept in an acid bath and post-annealing (e.g. thermal, chemical, and electrochemical), depending on the requirement of the study. Thermal annealing is a commonly used process for tuning the ligaments and pore size of np-Au. However, the effects of thermal annealing on modification of ligaments and gaps sizes are not completely understood and more research needs to be done. Herein, we have explored the effect of annealing time and thickness of the np-Au sample on modification of ligaments and gaps. Furthermore, we used the electroless plating method to cover the pores or gaps partially on the surface without modifying the interior of np-Au. As-prepared np-Au was then studied as a platform for molecular loading and releasing kinetics for the possible use in drug delivery. We have found that simply applying the electroless deposition for 1 to 5 min can drastically decrease the rate of release of the

molecules, and flow cell-based loading is the preferred way to load the molecules inside np-Au compared to the static method.

The structure of the np-Au monoliths before and after the modification was characterized using Energy-Dispersive X-ray Spectroscopy (EDS) and scanning electron microscopy (SEM), whereas the molecular loading and releasing studies were performed using UV-Vis spectrophotometer.

DEDICATION

To

MY FAMILY

ACKNOWLEDGEMENTS

Arif), all my sisters and my brother. They all wished that I could get my Master's degree

from the United States. Finally, I would like to express my deepest love to my respected and

caring husband and my lovely children for their understanding and support in every possible

way in these years.

"In this matter, and in all things, to God be the glory."

Table of Contents

Table of Figures

Modification and Utilization of the Nanoporous Gold for Loading and Release of Drugs

Ibtisam Al-badri, Keith J. Stine

University of Missouri–St. Louis, MO

Chapter 1   Introduction

Gold has been in use throughout the centuries because of its unique beauty and resistance to corrosion. Many ancient cultures started using gold for jewelry and ceremonial objects, and this is common even in modern time. In recent years, gold has been used extensively in electronics and other industries because of its remarkable qualities of conductivity, and its ability to resist corrosion. In particular, nanoporous gold (np-Au) offers a unique enhancement of the surface area which makes it especially useful in comparison to slabs or thin films of alloy or metal.[1] In the past decades, a growing interest in research and development has been devoted to np-Au not only because of the enhancement of surface area but also because of other unique features such as optical properties enhancement and thiol bonding-properties.[2-3] These properties make np-Au interesting to be used in a variety of current modern biomedical and industrial applications. Applications of np-Au include but not limited to immunoassays and sensors,[4-5] capture and separation of proteins,[6-7] study of

protein-carbohydrate interactions, [8-9] localized surface plasmon resonance [10-11], supported organic synthesis,[12-13] catalysis,[14] and energy storage[15].

The ligaments and gaps (pore size) of np-Au are features with considerable importance for the applications for which it is used. The width of the ligaments and pores of np-Au can be controlled and modified during or after the preparation of np-Au. The structure is typically created by the wet chemical corrosion method, wherein an alloy of gold is submerged into an acidic bath dissolving the less noble metals creating a nanoporous structure.[16] In this way, uniformly porous structures with pore size as small as 10 nm can be obtained. The resulting ligaments and pore size can be controlled by the time allowed in an acid bath and post-annealing techniques. Further research to effectively tune and predict the ligaments and pores size is essential for the use of np-Au in various applications.

1.1 Nanostructures and Nanopores of Metals

Nanostructures of metals can be prepared in varieties of shapes (e.g. spheres, cubes, stars, rods, tubes, films etc.), and different structures are suitable for different applications. Nanostructures of metals are classified as 0-,1-, 2-, and 3-D based on presence of at least one dimension having size around 1 to 100 nm.[17-18] An example of a 0-D nanostructure is a nanoparticle, whose three dimensions all are within nanometer range. If one of the three dimensions of the structure is not in the nanoscale range (long enough nanorods), the nanostructure is designated as 1-D. If two of the three dimensions are not in the nanoscale range (e.g., nanofilms), then it is classified as 2-D. Finally if none of the three dimensions of the material are in the nanoscale range, but the surface of any dimensions consists of nanoscale features, then the structure is called 3-D, example of which consists of

nanocomposites and nanocrystallites, Figure 1.[19] Monolithic nanoporous metals have all the

three dimensions that are not in the nanoscale. However, the widths of the ligaments in all the

three dimensions are in nanoscale range making them 3-D nanostructures according to this

classification. However, if only the nanoscaled features on the surface are considered,

repeating patterns of the ligaments and gaps make nanoporous metals 1-D like nanostructures

with the typical ligaments width less than 100 nm.
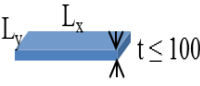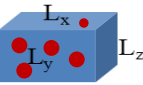
Dimensions	Nanoscale Dimension
0-D $\quad d \leq 100$	All the three dimensions at nanoscale e.g., nanoparticles
1-D $\quad d \leq 100 \quad L$	Two dimensions at nanoscale, L is not e.g., nanorods, nanotubes
2-D $\quad L_y \quad L_x \quad t \leq 100$	One dimension (t) at nanoscale, other two are not e.g., thin nanofilms
3-D $\quad L_x \quad L_y \quad L_z$	All the three dimensions are not at nanoscale e.g., nanocrystalline and nanocomposite materials

Figure 1.1 Classification of nanostructures based on dimensions. Reprinted with permission from
the Reference 19.

Nanoporous structures of the metals are noted for unique conductivity, high surface

area as well as the ability to absorb or scatter light because of large optical field

enhancements by noble metals.[20] They are also useful for thermal applications such as in heat exchangers, heat sinks, and heat pipes.[1, 21] Common examples of metals prepared in nanoporous form are gold, silver, copper, and zinc. Usually, the process of producing nanoporous metals begins with a metallic alloy, crystal or glass and then one (or more) of the less noble components is removed by chemical or electrochemical means. Kim & Nishikawa describe the production of nanoporous silver that was prepared from a melt-spun Al-Ag alloy using a hydrochloric acid solution to remove the aluminum to produce a uniform nanoporous Ag structure.[22] Similarly, Qi et al. describe the formation of nanoporous copper by removing the aluminum from Al_2Cu or AlCu alloys, using a NaOH or HCl aqueous solution.[23] Qi et al. showed that monolithic nanoporous copper (NPC) can be fabricated through electroless dealloying of Al-Cu alloys with a composition range of 33-50 at % Cu.[23-24] Moreover, they demonstrated that the uniform porous structure of NPC can be obtained from one or a combination of Al_2Cu and AlCu intermetallic compounds by dealloying with a NaOH solution. In addition, the porous structure of NPC can be modulated by simply changing the dealloying solution. The experiments produced a nanoporous copper ribbon that exhibited an open, bicontinuous interpenetrating ligament-channel structure. Dan, et al. describe the production of nanoporous copper from Ti-Cu alloy using hydrofluoric acid, rather than the more typical Al-Cu, Mn-Cu or Al-Zn-Cu precursors.[25] Liu et al. describe the production of nanoporous copper from a Mg-Cu precursor in HCl solution at room temperature.[26] They investigated the use of chemical dealloying of melt-spun dual-phase Mg with Cu (12 at. % Cu) alloy comprising α-Mg and Mg_2Cu phases in HCl solution at room temperature to fabricate monolithic NPC ribbons with ultrahigh specific surface area. Liu et al. determined that the dual-phase Mg alloy can be fully dealloyed resulting in the formation of uniform-

structured NPC ribbons with relatively large pore sizes compared to the ligament dimensions.[26] Current research is exploring the use of nanoporous zinc foam for anodes in batteries.[27] Raney nickel, developed by Murray Raney, is derived from a Ni-Al alloy and has been in use as a catalyst since the 1940s because of its high catalytic activity at room temperature [28] .

The generally used method of producing these nanoporous metals is to expose the binary or ternary alloy to an acid or a base bath. One of the elements of the alloy or intermetallic compound is then removed by the chemical dissolution process. Alternately, a component can be removed with the use of electrolysis in an electrolyte solution. The removal of one of the elements of the alloy leaves a nanoporous structure, with pores in the several to tens of nanometers depending on the preparation conditions. The different uses of porous metals depend on the pore sizes and morphology of each unique porous material. Although varieties of alloys and metals have been studied, this thesis will focus on properties and uses of np-Au. For general analysis, discussion of np-Au can be roughly divided into fabrication, characterization, and applications. These areas will each be briefly discussed in the following sections.

1.2 Fabrication of Nanoporous Gold

Nanoporous gold is a sponge-like structure of gold having pores (also referred to as interligament gaps) and interconnected ligaments, defined by their widths. When the less noble element in the precursor alloy, most typically silver or copper, is removed, the remaining gold forms into randomly shaped islands and these then transform into ligaments which become connected provided that the gold percentage is in the 20–50 at. % range. The

coarseness of the pores and ligaments depends on the method of production. The widths of the ligaments of nanoporous gold and the gaps between them generally range from a few nanometers to a few hundred nanometers.[29] Erlebacher et al. proposed a continuum model of the de-alloying process of a gold-silver (Au-Ag) alloy and pointed out that the nanoporosity formed upon dealloying of metals is due to an intrinsic dynamic pattern formation process, where the pores are formed because of the chemically driven aggregation of gold atoms in a phase separation process.[30]

The fabrication of np-Au is generally achieved by one of two processes: electrolytic techniques or selective dissolution, both also known as dealloying. Both processes begin with a sample of the precursor alloy. The electrolytic technique involves placing the sample in a diluted acid solution, usually perchloric acid , nitric acid, or potassium nitrate , and applying a controlled anodic potential. Detsi et al. experimented with an alloy of atomic percent composition $Au_{25}Ag_{75}$ and utilized 1 M perchloric acid to dissolve the silver using a three-electrode electrochemical cell.[31] The rate of silver dissolution was controlled by varying the applied potential between 0.8 and 1.3 V. They found that the rate of silver atom dissolution was higher at higher potentials. At 0.8 V it takes about 15 hours for silver dissolution, while at 1.3 V the same process can be completed in 1 hour. Seker et al. point out that the electrolytic method has more controllable parameters and results in finer porosity, but is not applicable for some situations.[31] The Okman group points out that electrochemical dealloying in acid solutions is a preferable alternative to free corrosion because it allows precise control over the potential and therefore provides better control over the Ag dissolution rate.[32] In contrast, in free corrosion the Ag dissolution rate is determined solely by electrolyte concentration and temperature. Crack-free np-Au leaves are produced while floating in a

neutral electrolyte, for which smaller pore sizes (< 10 nm) than those produced in free corrosion are reported. In other instances, dealloying by direct immersion in an acid bath for incremental lengths of time is used. Snyder et al. demonstrate that small fractions of Pt added to precursor Ag/Au alloys resulted in a new ultraporous metal upon dealloying, possessing a pore size peaked at less than 4 nm, a self-assembled core/shell structure with a Pt rich shell, and remarkable stability against coarsening due to the slow surface diffusion of Pt.[33] In addition to the composition of the precursor alloy, the strength and type of acid used in producing the np-Au and the length of exposure in the acid bath have measurable and important effects on the configuration of the nanostructure of the final product.

In either dealloying method, the dissolution reaction begins on the outer surface of the sample. In a gold and silver alloy, for example, as the silver is leached away, small islands of gold appear. Erlebacher et al. describe the process as starting when an atom of silver is dissolved and it leaves behind a terrace vacancy.[30] The Ag atoms coordinating to this vacancy now have fewer lateral neighbors and are consequently more susceptible to dissolution. This results in the terrace being stripped and leaving behind gold atoms with no lateral coordination. Before the next layer is attacked, and it begins to dissolve, the gold atoms diffuse and begin to agglomerate into random islands. This results in a surface comprised of two distinct types of areas: pure gold clusters and exposed areas of alloy susceptible to further dissolution. As more silver is dissolved, more gold atoms are released at the surface. As the gold continues to form clusters and as increasing areas are undercut as silver is dissolved, the process leads to pit formation and porosity. As the porosity forms, the decomposition is occurring on a three-dimensional non-uniform surface with continuously increasing surface area. The size of the pores and ligaments and the porosity structure are

influenced by the type of alloy used[34] and other factors such as the anodic potential, the type of acid used, the temperature of the solution, etc. The process of dealloying in acid results in a coarser porosity.

The shape and size of the interligament gaps and ligaments of np-Au depend on several factors. These include type of alloy and compositional ratio,[34] corrosive environment, dealloying time and the electrodeposition potential,[16] and de-alloying temperature [35].

Detsi et al. concluded that the relationship between the de-alloying potential and the structure size was linear in a potential range varying from 0.8 to 1.3 V and that low de-alloying potential resulted in larger diameter pores in relation to the ligaments and that higher potentials result in comparable ligament and pore size.[31] In further research, the same group confirmed that the layered morphology of nanoporous gold is related to microband structures in the precursors.[36] They concluded that the multilayer morphology in their np-Au is directly coupled to the layered texture development of the alloy precursor.

Once np-Au is formed, it can be further manipulated by the process of thermal or electrochemical annealing which promotes the surface diffusion of gold atoms. The width of inter-ligament gaps and ligaments can still be further tuned by annealing at different temperatures for different times[37] or by providing cyclic potential sweeps for different number of cycles in different electrolytic solutions[38] .

Annealing rates are related to the strength of ion adsorption and to the surface coverage, both of which vary with potential.[38] Detsi et al. reported that for np-Au produced by dealloying at a fixed potential, gap size and ligament width would not be equal.[39] Sharma et al. reported that when dealloying was carried out at higher potentials mean ligament width and gap size became smaller, becoming nearly 3.6 nm each.[38]

Thermal annealing is a commonly used process to improve the malleability of metal. When applied to np-Au, thermal annealing results in increased pore sizes, making the process useful when pore size and surface area are critical such as surface enhanced Raman spectroscopy, catalysts and hosting of biomolecules.[40] The surface diffusion of Au atoms increases with temperature and aids the annealing process. [38]

Sharma et al. indicate that surface diffusion of gold in electrolyte solutions plays a crucial role in the rate of annealing of np-Au.[38] Surface diffusion coefficients in electrolyte solutions are on the order of $10^{-14}\,cm^2\,s^{-1}$. When determined in a vacuum or air the diffusion coefficients are much smaller, on the order of 10^{-16} -$10^{-20}\,cm^2\,s^{-1}$[38] . The value of the diffusion coefficients also increases with increasing applied potential and with increasing temperature. Sharma et al. concluded that the dependence of surface diffusion coefficients on temperature, applied potential and the presence of adsorbed anions are all critical for understanding coarsening of rough gold surfaces, and it results in changes of surface topography and annealing behavior of np-Au.[38]

Blanckenhagen et al. examined the effects on direct surface modification, and investigated the diffusion constant on a polycrystalline gold surface in a temperature range from 300 K to 773K.[41] The porosity of all free standing np-Au structures decreases as the temperature increases.[40] Seker et al. compared np-Au annealed at 200°C, 300°C, and 400°C and found that annealing produces significant changes in film thickness and average pore size.[42] At 300°C, clearly distinguishable Au clusters form and the pore size increases dramatically. There is a decrease in thickness between 300°C and 400°C, which is not currently understood. The fully dense Au clusters are slightly larger, and the average pore size slightly decreased at 400°C; that is, at elevated temperatures, there are fundamental

changes in morphology evolution that are accommodated by thermally activated mechanisms, such as surface migration, creep, and interdiffusion.

The interligament gaps can also be increased in a controlled manner by electrochemical annealing. Sharma et al. compared surface annealing in different electrolytes after annealing using 50 oxidation-reduction cycles.[38] By providing cyclic potential sweeps for different numbers of cycles in different electrolyte solutions, and examining pore size every 5 sweeps, they concluded that the cycling can lead to substantial increases in mean inter-ligament gap and ligament width. The cycling results in a material in which the mean inter-ligament gap is larger than the mean ligament width.[38] They concluded that measuring the electrochemical surface area of the np-Au using the gold oxide stripping method provides a better approximation than does using a diffusing redox probe. Sharma et al. performed annealing with three different annealing electrolyte solutions: KCl, $NaNO_3$, and $NaClO_4$. Different results were obtained and related to the strength of anion adsorption on the gold surface and its effect on Au surface diffusion. They observed that the maximum annealing occurs in chloride solution, but with significant loss of gold into the solution as the complex ion. They suggest that electrochemical annealing may be a useful alternative to thermal annealing or immersion for long periods in acid.

The advantages of the electrochemical fabrication method of metal nanostructures over other techniques are that structures can be formed without the need of templates, surfactants or any other stabilizers that can introduce impurities[43-44].

1.3 Methods for Characterization of Nanoporous Gold

Nanoporous gold is very attractive because of its structure and porosity. The total surface area can be estimated by gas adsorption and electrochemical methods such as electrochemical impedance spectroscopy[45] and formation and reduction of a monolayer of gold oxide.[38]

Characterization of nanoporous gold or other related materials can also be carried out using scanning electron microscopy; gas adsorption measurements of surface area (followed by fitting to an adsorption isotherm such as the Langmuir or Brunauer-Emmett-Teller (BET) or other models); thermogravimetric analysis and electrochemical methods for surface area.

One common method for characterizing nanoparticle surface coatings is electron microscopy, including scanning electron microscopy (SEM) and transmission electron microscopy (TEM). Electron microscopy can be used to measure ligament and gap sizes and uniformity. Electron microscopy can be used to evaluate the presence of nanoparticle coatings on dried nanoparticles and can be paired with secondary detectors to allow for elemental composition analysis.[46] It can require tedious work, to prepare the sample for imaging, and then gaining meaningful statistics and understanding the data.

Gas adsorption methods include the measurement of the adsorbed amount of N_2 gas as a function of N_2 partial pressure at 77 K, done for both increasing and then decreasing partial pressure to obtain an isotherm adsorption branch followed by a desorption branch. Other gases such as Krypton can be used to measure smaller surface areas but are not as commonly used.[47] Analysis of the surface area is often done using the Brunauer-Emmett-Teller (BET) method and the pore size distribution is then found using the Barrett-Joyner-Halenda (BJH) analysis. BET analysis provides precise specific surface area evaluation of

materials. This method was proposed by Brunauer, Emmett and Teller and it is based on the following assumptions: the adsorbent surface is homogeneous, the adsorbent-adsorbate interaction is stronger than the adsorbate-adsorbate interaction, the interaction of adsorbed molecules is considered only in the direction perpendicular to the surface, and is regarded as condensation.[48] It utilizes nitrogen multilayer adsorption measured as a function of relative N_2 pressure, P/P_0 where P_0 is the vapor pressure of N_2 at 77 K and P/P_0 is varied between 0 and 1. The technique encompasses external area and pore area evaluations to determine the total specific surface area in m^2/g yielding important information in studying the effects of porosity and particle size in many applications. The method of Barrett-Joyner-Halenda (BJH), proposed in 1951, was originally designed for relatively wide-pore adsorbents with a wide pore size distribution. However, it was repeatedly demonstrated that it can be successfully applied to virtually all types of porous materials. The model is based on the assumption that pores have a cylindrical shape and that pore radius is equal to the sum of the Kelvin radius and the thickness of the film adsorbed on the pore wall.[49]

Each of these procedures is applied shortly before electrochemical measurements or derivatization steps are carried out, in view of the reactive nature of the cleaned gold surface for adsorbing contaminants from the atmosphere. Most electrochemical procedures share a common step, i.e., an oxidative treatment to decompose and remove adsorbed material, and to form a hydrophilic layer of gold oxides on the surface, which can then be reduced back to gold producing a clean gold surface. Chemical oxidation with piranha solution (a mixture of concentrated H_2SO_4 and H_2O_2) and treatment in an oxygen plasma or with ozone are frequently applied.[50-51] In some procedures, a thin layer of gold is removed by the action of aqua regia (a mixture of hydrochloric and nitric acids). After oxidation, a subsequent

reduction of the formed gold oxide has been reported to be necessary to obtain SAMs with a good quality. This can easily be performed by, for instance, immersion in ethanol. For example, Ron and Rubinstein found that 10 min in ethanol is sufficient to completely reduce the gold oxide produced by 6 min of plasma oxidation.[52] Sharma et al. describe the use of multiple cycles of cleaning the surface with sulfuric acid (H_2SO_4).[38] They observed that two sequential oxide-stripping scans in H_2SO_4 revealed no change in the appearance of the np-Au structure. Other research by Dong and Cao indicated that large numbers of scans, 100–200, may result in coarsening of the material.[53]

Thermogravimetric analysis (TGA) is a straightforward analytical technique that typically requires no special sample preparation beyond drying of the sample. Research has shown that TGA can be reliably used to evaluate the purity of and characterize nanomaterials.[54] For thermogravimetric analysis, materials are heated to elevated temperatures while monitoring the mass of the sample, which yields the decomposition curve. Analysis of the decomposition curve yields the oxidation temperature and residual mass of the sample.[46] The use of TGA was also described by Tan et al. to determine the mass of organic molecules on the surface of np-Au samples after dealloying.[55] They found TGA analysis to be a very suitable method for determining surface loading of SAMS inside np-Au monoliths of sufficient size. The group found that the sensitivity of TGA for mass changes on the surfaces of the monoliths of the size used in this study is comparable on a per unit area basis.

1.4 Applications of Nanoporous Gold

Nanoporous gold is of much interest to scientists because of its high surface area-to-volume ratio, ease of preparation and modification, biocompatibility, conductivity, chemical and physical stability, and regenerative nature.[56] Some documented use has been described from very early periods in some very early cultures. Erlebacher et al. briefly mention the use by early Andean goldsmiths to enhance the surface of gold alloy objects by the method of selection dissolution of the copper constituent of the alloy.[30] More recent demands for gold for technological use in the biomedical and electronic industry have resulted in continued interest in research and analysis.

The modern study and application of np-Au is a relatively new phenomenon. Lefebvre et al. describe the research into the commercialization of the related but distinct materials known as metallic foams as active in the 1950s in the USA for a period of about ten years.[57] They mention that the second surge in the commercial research and development took place in the 1990s. Since the late 1990s, there has been sufficient interest to conduct a biennial conference, Metafoam, to discuss foamed metals in general. Seker et al. also document the recent surge of interest in the uses and production of np-Au in particular.[58] This surge of interest is exemplified by the publication of about 25 scientific papers concerning np-Au in the period from 1992 to 2005, which increased to more than 80 papers in the period between 2006 and 2009 and continues to increase to the present. Seker et al. in 2009 stress that there are still many underexplored features of this material, including surface functionalization and biological applications.[58] Dixon et al. in 2006 describe the high interest in np-Au, in particular, because of the rich electromagnetic responses of gold nanostructures including planar thin films, periodic gratings, roughened surfaces and nanoparticle arrays and

the ability of np-Au surfaces to support self-assembled monolayer functionalization chemistry.[59] The nanoporous structure has a surface area at least 100 times higher than planar gold of an equivalent geometric area, which makes it more useful in a variety of applications.

Weissmüller et al. demonstrated that nanoporous metals exhibit actuator characteristics because they have a large surface-to-volume ratio and considerable charge induced on their surface.[60] Nanoporous gold has been used as a surface chemistry driven actuator converting chemical energy into a mechanical response.[43] Biener et al. demonstrated that surface-chemistry-driven actuation can be realized in high-surface-area materials such as np-Au [43]. They achieved reversible strain amplitudes of the order of a few tenths of a percent by alternating exposure of np-Au to ozone and carbon monoxide. The effect can be explained by adsorbate-induced changes of the surface stress.

Wang et al. described the controlled synthesis of dendritic Au/Pt core–shell nanomaterials for use as effective fuel cell electrocatalysts.[61] Yan et al. researched the use of np-Au in a direct liquid hydrazine/hydrogen peroxide N_2H_4/H_2O_2 fuel cell (DHHPFC).[62] DHHPFCs are known to be a unique power source for air-independent applications under extreme conditions such as outer space and underwater environments. Yan et al. found that working as both anode and cathode catalysts, nanoporous gold leaf was found to be able to power a fuel cell with a specific power at least one order of magnitude higher than that of Pt/C under the same testing conditions. They demonstrated that dealloyed np-Au in a freestanding leaf form (np-AuL) can function as a novel electrocatalyst on both anode and cathode in a hydrazine/hydrogen peroxide fuel cell. This is due to np-AuL's intrinsically high electrocatalytic activities toward N_2H_4 oxidation and H_2O_2 reduction, a behavior not readily seen on planar Au electrodes.

Pornsuriyasak et al. studied the use of np-Au as a new surface-tethered iterative carbohydrate synthesis (STICS) technology.[63] They prepared a surface functionalized 'stick' made of chemically stable high surface area porous gold, which allowed cost efficient and simple synthesis of oligosaccharides. At the end of the synthesis, the np-Au stick could be reused for subsequent syntheses after the oligosaccharide was removed. Ganesh et al. demonstrated the use of STICS using an HPLC assisted setup.[64] They took freshly dealloyed np-Au and placed it in a solution of lipoic acid conjugated glycosyl acceptor and lipoic acid methyl ester under argon for ten hours. The loaded chips were then transferred to the column connected to an HPLC system to use in subsequent glycosylations. They demonstrated that the use of mixed SAMs helps to provide the required space for reaction around the immobilized spacer. The glycosyl acceptor with the longer spacer had a higher tendency to mimic a solution phase reaction environment than that of acceptors with shorter spacers.[64] Tan et al. demonstrated functionalization, resistance to non-specific adsorption, stability under flow conditions, selectivity in protein binding, and successful elution of protein.[7] The portable nature of np-Au monoliths, their size and shape flexibility, and the fact that monoliths bearing different surface modifications can be arranged in sequences within flow systems, suggests the possibility of their use in modular systems for biomolecule separation, controlled release, or selective capture.

Nanoporous gold has been used as a catalyst in several applications including for carbon monoxide oxidation at low temperature,[14] reduction of oxygen to water,[65] and aerobic oxidation of D-glucose to D-gluconic acid [66]. Deronzier et al. demonstrated that compared with metallic Au or Ag catalysts, the np-Au alloy catalysts exhibited high activity toward CO and/or H_2 oxidation and exceptionally high selectivity at low temperature for CO oxidation in

the presence of H_2 showing a synergistic effect between Au and Ag.[67] Deronzier et al. conducted low-energy ion-scattering experiments which provided composition data about the topmost atomic layer, i.e., where catalytic reactions occur and allowed them to establish a clear correlation between top layer surface concentration and reactivity.[67]

Hu et al[68] experimented with a sensitive electrochemical DNA sensor based on nanoporous gold (np-Au) electrode and multifunctional encoded Au nanoparticles (AuNP). A DNA biosensor was fabricated by immobilizing capture probe DNA on the np-Au electrode and hybridization. They took advantage of the dual-amplification effects of the np-Au electrode and multifunctional encoded AuNP, this DNA biosensor could detect the DNA target quantitatively, in the range of $8.0 \times 10^{-17} - 1.6 \times 10^{-12}$ M, with a limit of detection as low as 28 aM, and exhibited excellent selectivity even for single-mismatched DNA strand detection. np-Au has also been used in biomedical applications as a biosensor in glucose systems detecting glucose and protein in urine[69] and multiple other biological applications[7, 58, 70].

Hu et al[68] have shown for that the unsupported AuNPore catalyst is an efficient heterogeneous catalyst for the selective semihydrogenation of alkynes, whereas the unsupported gold was so far known to be inactive for hydrogenation.[71] Moreover, the AuNPore catalyst is easily recoverable and can be reused several times without leaching and loss of activity.

Recent research has shown np-Au to be useful in the immobilization of various enzymes. Some examples are studies of laccase[72] bilirubin oxidase and lipase and catalase[73]. Stine group described the use of np-Au for enzyme immobilization.[59] They found that covalent enzyme immobilization could be achieved by first forming a self-assembled

monolayer on np-Au bearing a terminal reactive functional group followed by conjugation to the enzyme through amide linkages to lysine residues.[67]

Nanoporous gold can also be used in applications requiring measured release of molecules. In order to study the effect of thin film morphology on release kinetics,[74] investigated the release properties of np-Au samples of varying thickness. They also examined the effect of pore size and general morphology. In their study, they demonstrated that the drug loading capacity and the release kinetics of np-Au thin films could be tuned by modulating np-Au film thickness and morphology.[74]

1.5 Electroless Deposition of Gold

Electroless deposition is a process of depositing a coating with the aid of a chemical reducing agent in solution and without the application of external electrical power.[75] The basic electroless deposition process is as follows: electrons derived from heterogeneous oxidation of a reducing agent at a catalytically active region of the surface reduce metal ions to metal atoms, which deposit on the surface. Under the right conditions with a prepared surface, a continuous film is deposited.

The term electroless plating, originally used to refer to only an autocatalytic process, is now used to refer to three types: autocatalytic; galvanic displacement; and substrate-catalyzed processes.[76-77] Galvanic displacement, or immersion, uses no reducing agent in the bath formulation; autocatalytic and substrate-catalyzed processes both include a reducing agent in the solution. In autocatalytic deposition, the process continues indefinitely, resulting in a thick layer of deposited gold. Okinaka and Kato indicate that electroless plating has, in

principle, a distinct advantage over electroplating in its capability of minimizing the number of processing steps when gold is needed in areas electrically isolated from each other.[78]

In electroless plating on substrates, the reaction is substrate catalyzed or galvanic displacement. Okinaka stated that the electroless plating of gold on noble metals such as Pd, Rh, Ag and Au itself are catalytic while the gold plating on active metals such as Cu, Ni, Fe, and their alloys is initiated by galvanic displacement.[79]

A displacement reaction occurs when an ion of a less active metal is reduced and deposits on top of a more active metal, which is oxidized. During galvanic displacement processes generally no reducing agent is present in the bath formulation[80] researched gold deposition by galvanic displacement on semiconductor surfaces and the effect of substrate on adhesion. They studied thin gold films grown on Si and Ge substrates by galvanic displacement from fluoride-containing solutions. They concluded that displaced gold films exhibit strong adhesion to germanium substrates but not to silicon because of a chemical bond at the Au-Ge interface. Srikanth and Jeevanandam studied the differences in galvanic displacement and electroless methods for deposition of gold nanoparticles by depositing gold nanoparticles on synthetic calcite using two different methods: electroless deposition and galvanic displacement reaction.[81] They explained that in the galvanic displacement reaction, the replacement of Ag by Au is based on their reduction potentials. The standard reduction potential for Ag^+/Ag system is +0.767 V, while that for Au^{3+}/Au is +0.995 V. Due to the higher reduction potential of Au^{3+}/Au system, the Au^{3+} ions are reduced to Au on calcite with the concomitant oxidation of Ag to Ag^+. They concluded that surface modification is necessary for uniform deposition of gold nanoparticles. During the galvanic displacement reaction, when displacement of silver with gold takes place, there is no control on the size of

the deposited Au nanoparticles, which results in a larger particle size. Moreover, electroless deposition leads to the formation of uniform, smaller and well separated gold nanoparticles compared to the galvanic displacement reaction. They concluded that electroless deposition is better for a uniform deposition of smaller Au nanoparticles on calcite compared to the galvanic displacement reaction.[81]

Autocatalytic and substrate catalyzed processes both contain a reducing agent. The reducing agent acts as a catalyst to initiate the chemical reaction with the substrate. In the borohydride solution the BH_4 does not act as a catalyst, but intermediate borohydride compounds which are formed act as catalysts on the surface.[79] Researchers have experimented with many bath compositions to enhance the process, and perform in different temperature ranges and alkaline vs acidic conditions, depending on the type of substrate used[79].

Electroless plating can be used to deposit gold/silver alloys. Au-Ag alloys can be plated by operating the borohydride gold bath with the continuous addition of $KAg(CN)_2$ and excess cyanide.[79] Au-Cu alloy can be plated by adding $Au(CN)_2^-$ to the conventional electroless copper plating bath containing EDTA and formaldehyde.[79] This results in a deposition of homogeneously mixed crystals of copper and gold with a characteristic lattice formation in contrast to Au-Cu deposited with the conventional electrodeposition method[79] Au-Sn alloys can be plated using stannous chloride as the reducing agent.[79, 82]

Okinaka and Kato have also reported the experiments conducted to improve the effectiveness of the conventional borohydride and dimethylamine borane (DMAB) baths. The conventional borohydride bath has a utilization efficiency under typical plating conditions of only 2-3%.[78] The multistep chemical reaction is very dependent on maintaining

a stable KOH concentration. The reaction rate increases with decreasing KOH concentration but concentration must stay greater than 0.1 M to prevent spontaneous decomposition of the bath. In a DMAB bath, the KOH concentration is also critical but opposite to the borohydride situation. In the DMAB bath, the rate increases with KOH concentration. The plating rate can be increased by agitation, increase in gold concentration and temperature.[79] In practical terms, Okinaka and Kato sum up the problems of using borohydride and/or DMAB as: the plating rate is low; bath stability is insufficient; baths are sensitive to contamination with minute amounts of nickel; a high pH is required and the baths contain free cyanide.

Research by Paunovic and Sambucetti experimented with a variety of non-cyanide baths determined that a sulfide-thiosulfate mixed-ligand system combined with hypophosphate gave the most satisfactory performance for plating rate and bath stability.

Molenaar describes the autocatalytic deposition of gold-copper alloys from an alkaline solution containing formaldehyde, gold cyanide and copper ions in an ethylenediaminetetraacetic acid (ETDA).[83] Molenaar studied in the presence of cyanide ions, the oxidation of formaldehyde, which provides the electrons for the Au-ion reduction, can only occur on a Cu-containing surface. This technique enabled deposits with gold content ranging from 5 to 99 percent[83].

Both the composition and the rate of the deposited gold are influenced by the composition of the bath. Iacovangelo & Zarnoch describe the use of hydrazine as a reducing agent in an electroless gold plating formulation.[84] They demonstrated that excess free cyanide can be used to stabilize the gold cyanide complex and allows "substrate-catalyzed," plating which is neither immersion nor autocatalytic plating. This bath plates of pure gold films at high initial rates up to 10 μm/h with exceptional bath stability and life.[79] It was found

that gold deposited over base metals using a hydrophosphite bath was porous and that the diffusion of the substrate metal to the gold surface occurs readily. Okinaka stated that the composition of gold-copper alloy can be varied from 5.8% gold to 99% gold can be varied by varying the amount of $KAu(CN)_2$ in the bath.[79] The higher the concentration of $KAu(CN)_2$ in the bath the higher the percentage of gold.

Chapter 2   Modification of Nanoporous Gold

2.1 Experimental Methods

2.1.1   Dealloying

 Commercially available 0.5 mm and 0.25 mm thick, ten-carat yellow gold plates (41.7% Au, 20.3% Ag, and 38.0% Cu) and 200 nm gold leaf were cut into a nominal size of 2 mm $\times$ 2 mm. The cut gold plates/leaves were dealloyed by placing in a concentrated nitric acid bath for 12 h, 24 h, and 48 h. Fresh nitric acid was replaced after 24 h for 48 h dealloying. Gold leaf was handled using a homemade platinum ring. The dealloyed plates/leaves were rinsed thoroughly with Milli-Q wat-er then rinsed with ethanol. The monoliths were dried inside a vacuum desiccator until being used.

2.1.2   Thermal annealing of np-Au monoliths:

Dried np-Au monoliths were annealed inside the oven at desired temperature 300°C for different times: 1h, 2h, and 3h.

2.1.3   SEM and Energy Dispersive X-ray Spectroscopy (EDS)

The exterior and interior microstructure of np-Au monoliths were characterized using SEM at accelerating voltage 5 kV and working distance 8 mm. The elemental analysis was done using the EDS detector attached to SEM.

2.1.4   ImageJ

The ligament width and interligament gaps (pore size) were analyzed using ImageJ digital image analyzing software. The analysis was performed by dividing each image into

four quarters and taking ten measurements from each quarter for both ligament width and interligament gaps.

2.2 Results and Discussion

Dealloying conditions are very important in the formation of structures of nanoporous gold. The shape and size of the interligament gaps and ligaments of np-Au depend on several factors. These include type of alloy and compositional ratio,[34] corrosive environments, dealloying time, the electrodeposition potential,[16] and dealloying temperature[35]. Figure 2.1A show the typical dealloying set up containing beaker with nitric acid and Figure 2.1B-D show the photographic image, SEM image, and EDS spectra of np-Au after dealloying, respectively. In this work, we will explore the effect of the volume of nitric acid, dealloying time, thickness of alloy, and post annealing time on the modification of np-Au.
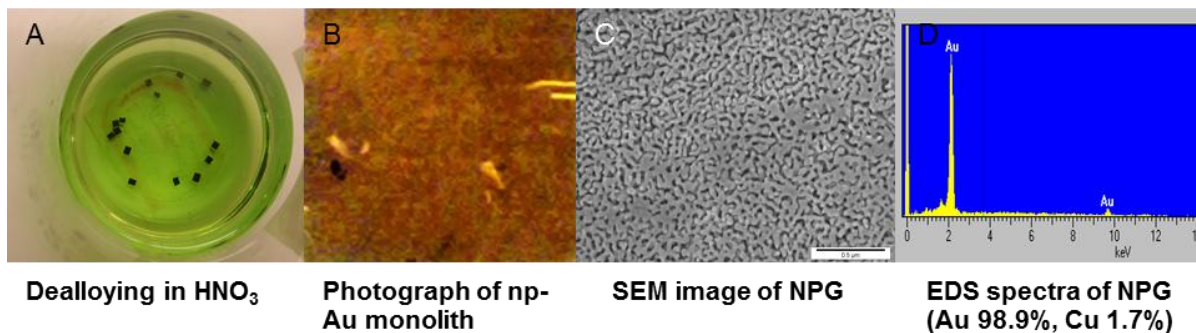
Figure 2.1. A) Typical dealloying setup for preparing np-Au, B) photographic image of NPG prepared after 48 h dealloying, C) SEM micrograph of np-Au, and D) EDS spectrum showing composition of gold and remaining copper.

2.2.1 Effect of volume of nitric acid on np-Au structure

The effect of the volume of nitric acid to nanoporous structure was tested by dipping gold plates in nitric acid, per plate in either 0.25 mL or 5 mL volume of nitric acid. The SEM images of 0.25 and 0.5 mm thick gold plates dealloyed for different time at 0.25 mL/plate are

24

shown in Figure 2.2. As expected, it can be seen that with the increase in dealloying time, the ligament width and interligament gaps increases. The increase in dealloying time can help nitric acid to penetrate the entire precursor and provide stress for longer time giving the 3D nanoporous structure[85]. However, due to the incomplete dealloying at 12 h, random structures can be seen with larger ligament width at some regions and smaller at other regions. The results of elemental analysis (Figure 2.3 and 2.4) show that 0.25mL/plate dealloyed np-Au does not get completely free from less noble copper metal. In both 0.25 and 0.5 mm thick gold plates, it can be seen that even after 48 h of dealloying nearly 10% of copper element remains in the porous structure and is more than 10% for up to 24 hours of dealloying.

Therefore, for the complete removal of less noble metal, the volume of nitric acid should be excess and hence we changed the dealloying volume from 0.25 mL/plate to 5 mL/plate.
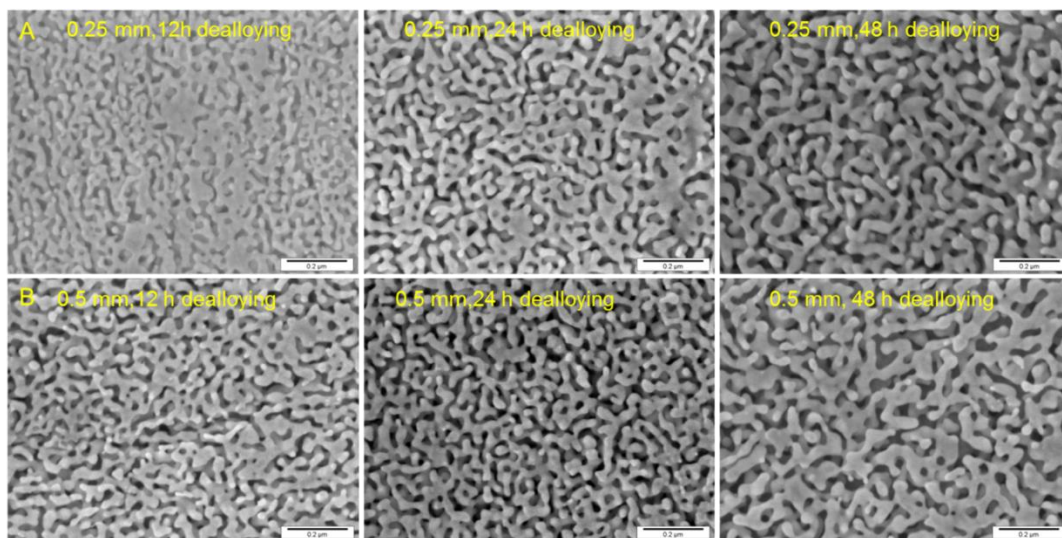
Figure 2.2. SEM images of the exterior morphology of np-Au monoliths having two different thicknesses. Row A) 0.25 mm and Row B) 0.50 mm, dealloyed at 12 h, 24 h, and 48 h. Scale bar = 200 nm.
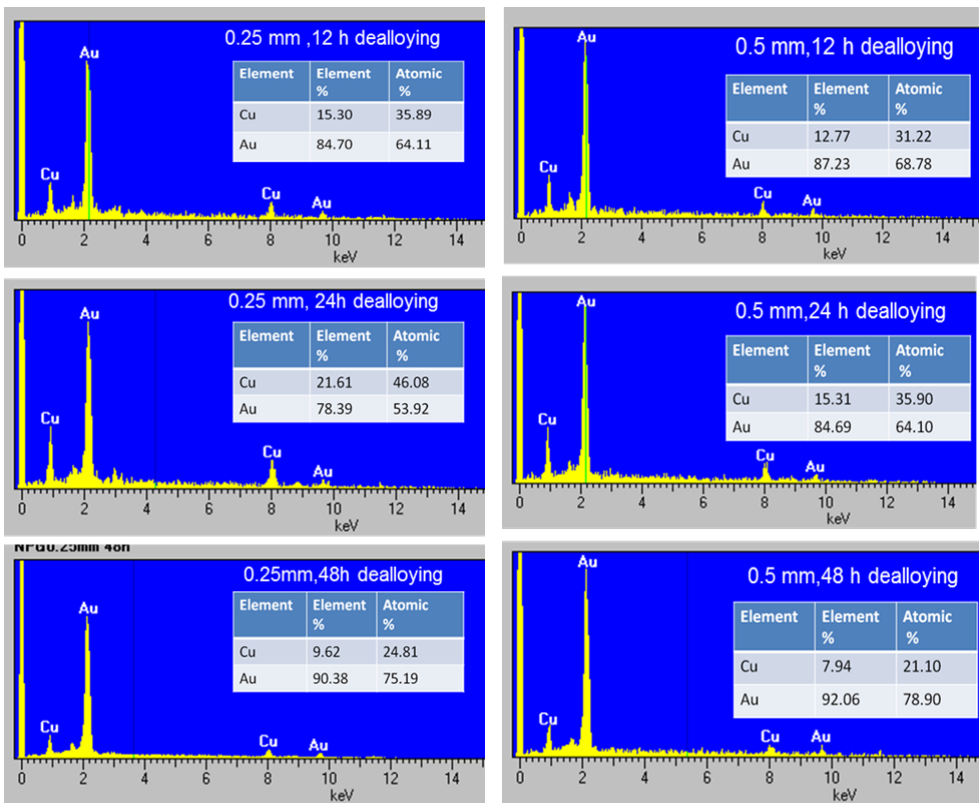
Figure 2.3 EDS spectra and percent composition of 0.25 mm and 0.50 mm thick np-Au monoliths dealloyed in 0.25 mL HNO_3 per plate (10 plates in 2.5 mL) for 12 h, 24 h, and 48 h.

We did not find any structure and composition changes when we prepared np-Au by dipping 20 plates in 100 mL solution versus 1 plate in 100 mL solution which helps us conclude that 5 mL nitric acid per plate condition is optimal for removal of less noble metal from gold to prepare np-Au. Figure 2.4 shows the exterior morphology of np-Au plates/leaves after dealloying in 5 ml of nitric acid per plate. It is clear that with the increase in dealloying time both the ligament width and interligament gaps increases for plates and leaves, which is due to the diffusion of gold metal under the stress of nitric acid. It was also observed that even though the change in morphology of np-Au plates having thickness very close for 0.25 mm versus 0.50 was not obvious, but when compared to thinner np-Au leaf (200 nm) the ligament width and interligament gaps changes drastically. The interior

26

morphology of np-Au plates are shown in Figure 2.5, whereas because of very thin layer of leaf it is difficult to take its SEM images and is not of much interest, so not taken. The ImageJ analyzed data to obtain the ligament width and interligament gaps are shown in figure 2.6. It is found that ligament widths in general are bigger than the interligament gaps. The most noteworthy information is the difference in ligament width and interligament gap between thicker plates and thinner leaves. The ligament width of the plates is around 30 nm, whereas the np-Au leaf prepared under the same condition (48 h dealloying) have ligament width around 56nm with higher standard deviation. Similarly, interligament gaps for plates are also nearly double from around 18 nm to 31 nm.

The average ligament width of the 0.5 mm plates dealloyed for 12 h is 20.5 ± 5.9 nm (n = 40) and the average of inter-ligament gap is 13.7 ± 3.72 nm (n = 40). For the 24 h dealloying the average ligament width is 20.8 ± 6 nm (n = 40) and the pore size is 13.9 ± 3.7 nm (n = 40), whereas for 48 h dealloying the ligament width becomes 22.24 ± 6.83 nm (n = 40) and pore size becomes 23.13 ± 7.7 nm (n = 40). Similarly, for 0.25 mm thick plate dealloyed for 12 h the average ligament width is 22.6 ± 9 nm (n = 40) and the average of pore size is 15.7 ± 4.5 nm (n = 40). After dealloying for 24 h the average ligament width becomes 27.8 ± 12.9 nm (n = 40) while the average pore size becomes 16.3 ± 4.13 nm. However, when dealloyed for 48 h, the average ligament width become 30.9 ± 7.3 nm (n = 40) and the average of pore size become 24.2 ± 7.11 nm (n = 40). Dealloying gold leaf of 200 nm for 12 h gives the average of ligament width of 23.8 ± 7.44 nm (n = 40) and the average pore size 19.5 ± 4.5 (n = 40). After 24 h dealloying, the average ligament width becomes 38.14 ± 14.8 nm (n = 40) and the pore size becomes 31.9 ± 10.13 nm (n = 40).While the

average of ligament width and pore size become 55.6 ± 22.5 nm and 31.01 ± 10.33 nm (n =
40), respectively after dealloying for 48 h.
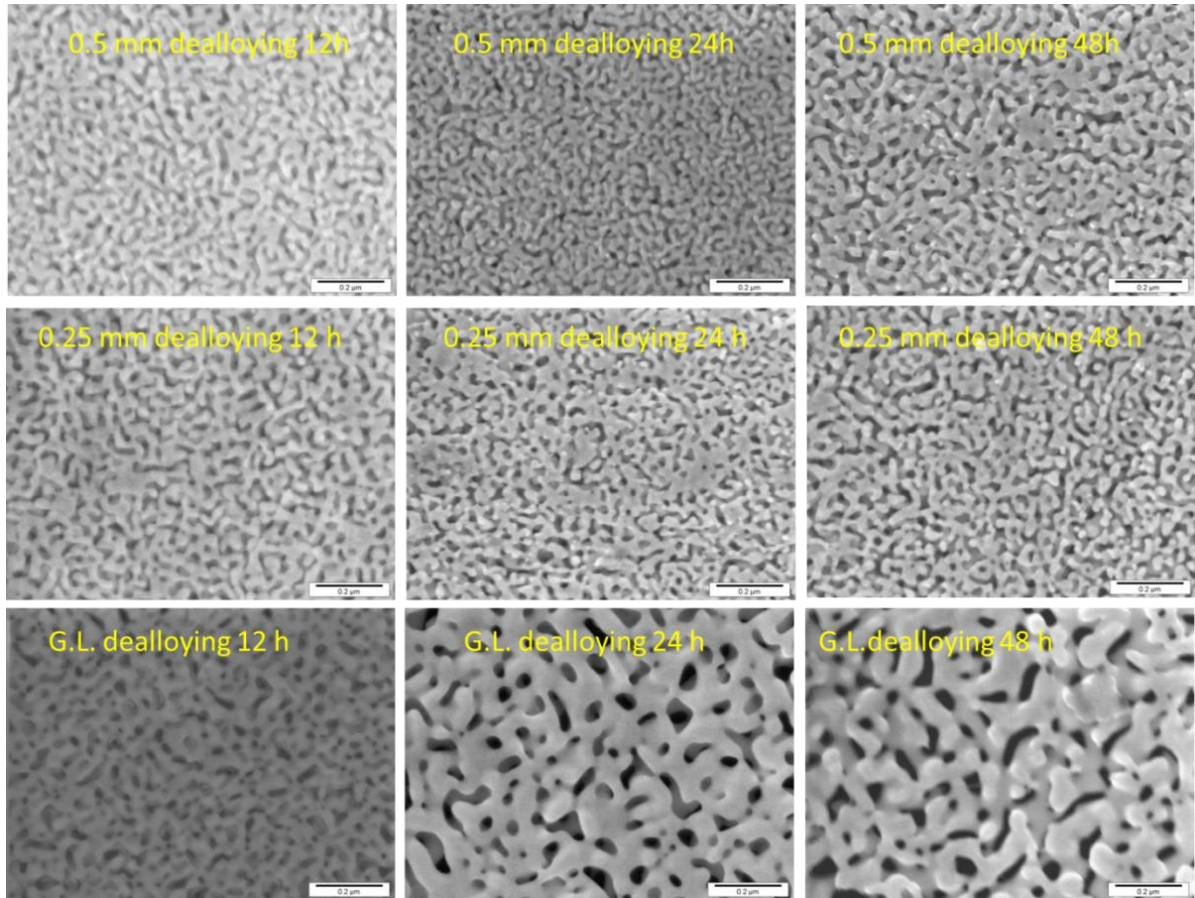
Figure 2.4 SEM images of the exterior of the np-Au of different thickness (0.5 mm, 0.25 mm, and gold leaf (200 nm) dealloyed in HNO_3 at different times. Small morphology changes for np-Au observed between 12 h and 24 h dealloying, and 0.5 mm and 0.25 mm thick. All scale bars = 0.2μm.
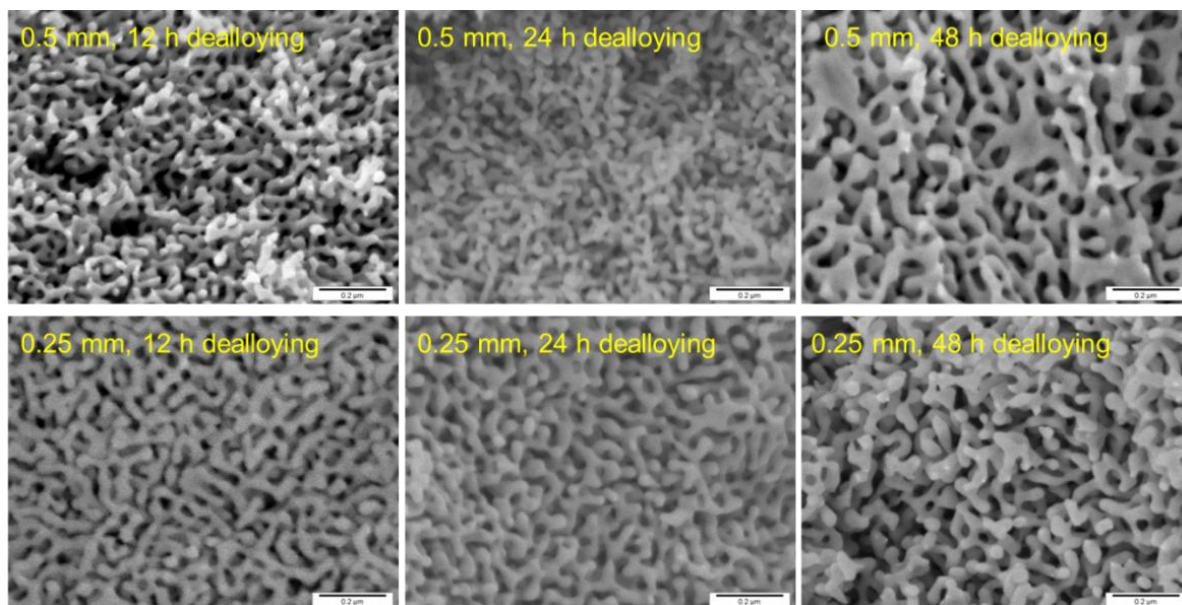
Figure 2.5 SEM images of the interior of np-Au in different thickness 0.5 mm and 0.25 mm dealloying in 100 ml concentrated HNO_3 at different times: 12 h, 24 h, and 48 h. All scale bars = 0.2μm.
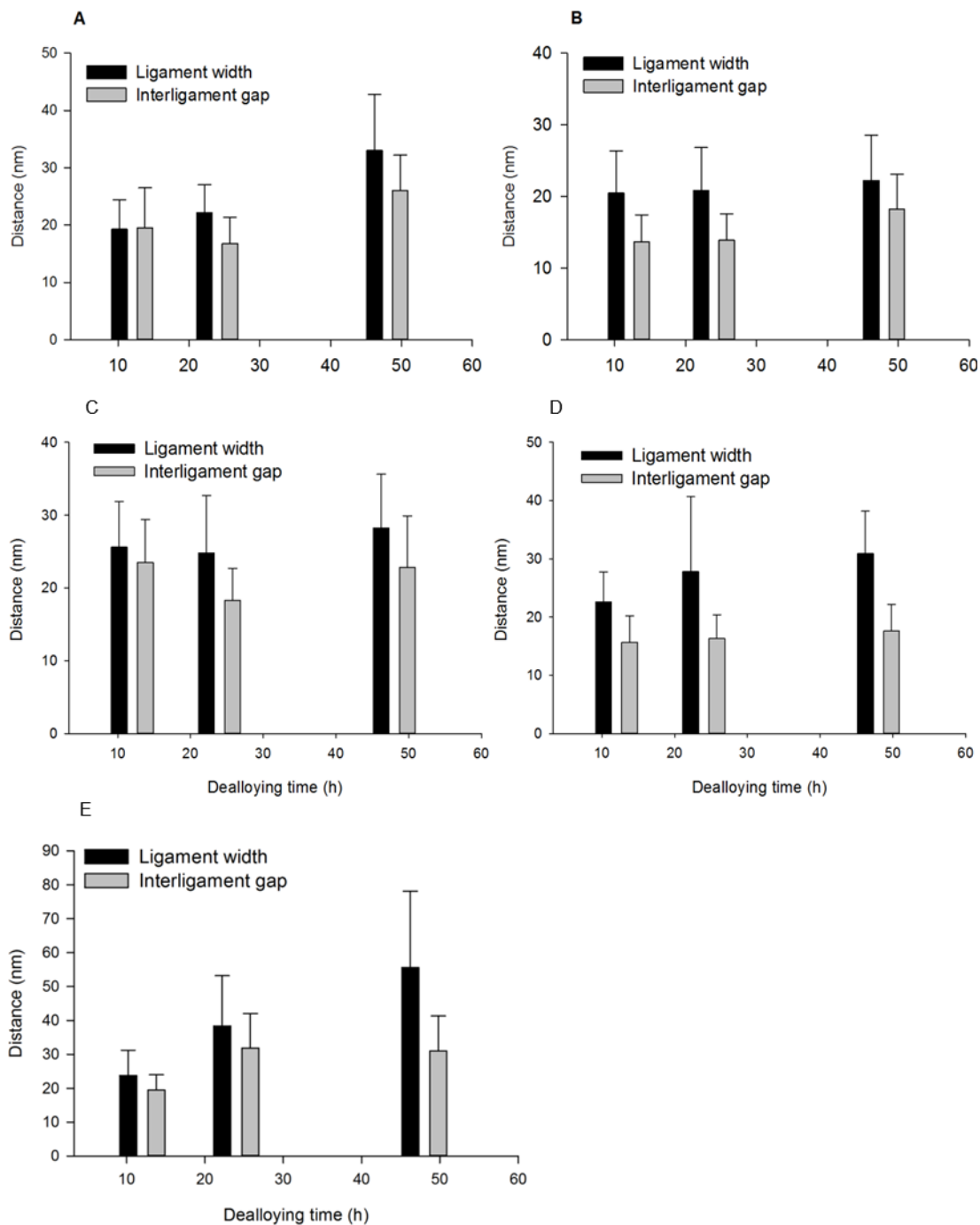
Figure 2.6 Histogram showing changes in ligament width and interligament gap of 0.5 mm (A, B), 0.25 (C, D) and 200 nm thick (E) np-Au, dealloyed at 12, 24, and 48 h. (A, C) interior analysis and (B, D, E) exterior analysis

Figure 2.7 represents the EDS spectra of np-Au of 0.25 and 0.5 mm thick plates. Unlike the np-Au prepared at 0.25 mL of nitric acid per plate, 5 mL of nitric acid per plate condition removes more than 97% of less noble elements within 12 hours. These results show that excess volume of nitric acid is critical for the removal of less noble metals. Providing the excess volume, the dealloying time can be drastically decreased while properly removing the less noble metals. In case of the gold leaf (Figure 2.8), there is no recordable presence of copper element within 12 hours of dealloying. Since the leaf was supported on glass, the background signals of Na, O, Si, and K are from glass. It is interesting to note that with increasing the dealloying time to prepare np-Au, the leaf is more penetrable by the beam of electron so the ratio of intensity of silicon to gold is less than 1 for 12 h, nearly 1 for 24 h and greater than 1 for 48 h.
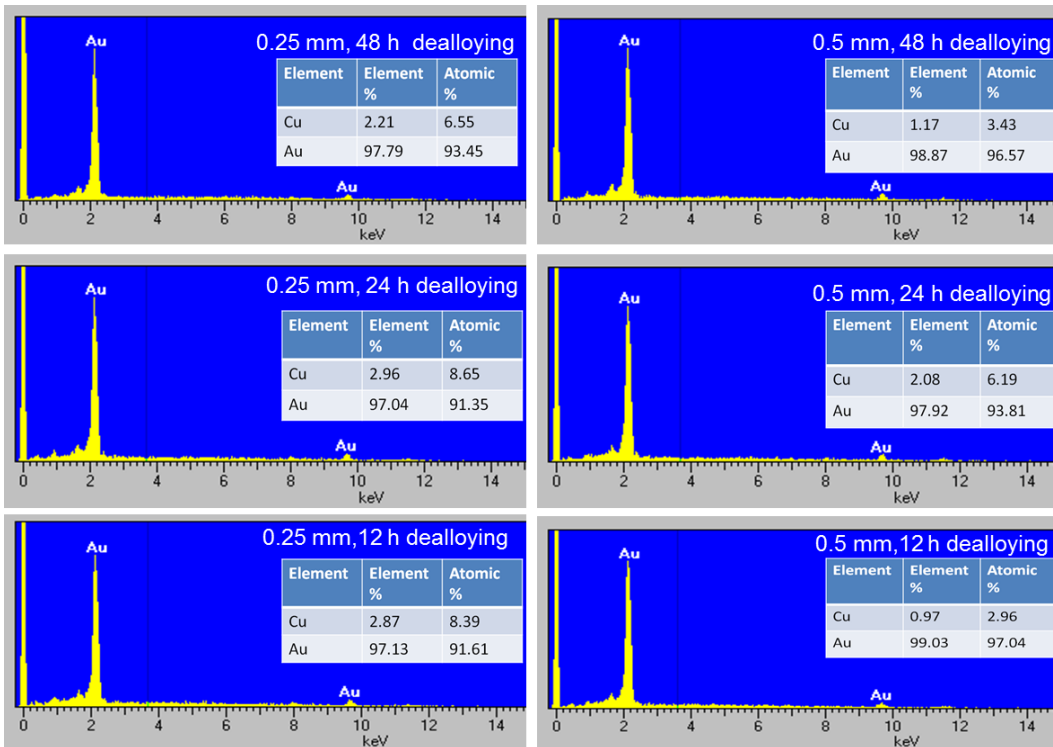
Figure 2.7 EDS spectra and percent compositions of 0.25 mm and 0.5 mm np-Au monoliths dealloyed for 12 h, 24 h, and 48 h in HNO_3.
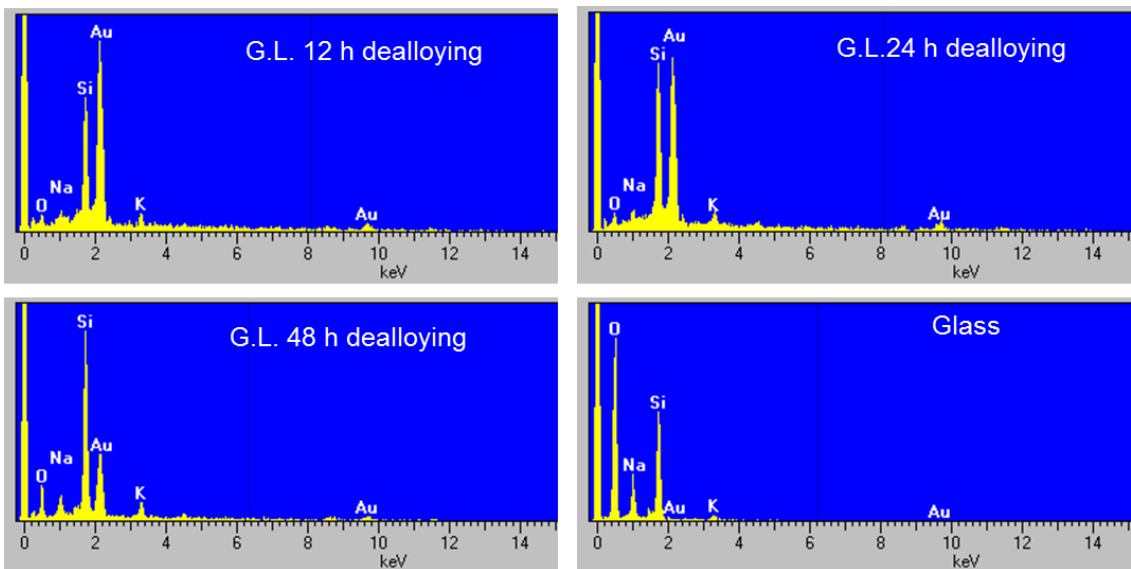
Figure 2.8 EDS spectra of gold leaf dealloyed in HNO_3 for 12 h, 24 h, and 48 h. Lower right represent the EDS spectra of glass (blank).

2.2.2   Thermal annealing

By thermal annealing, the ligaments width and interligament gaps of np-Au monoliths can be easily tuned.[40, 42] Study of np-Au annealed at 200, 300, and 400°C has found that annealing produces significant changes in film thickness and average pore size. At 300°C, clearly distinguishable Au clusters are formed and the pore size increases dramatically. To compare between ligament width and interligament gap of exterior and interior structure, here we studied np-Au of different thickness 0.5 mm, 0.25 mm, and gold leaf prepared at different times, 12 h, 24 h, and 48 h, using different annealing times, 1 h, 2 h, and 3 h at 300°C. Figure 2.9 shows SEM images of 0.5 mm thick np-Au prepared at different dealloying and annealing time. It has already been shown before that with increase in dealloying time the ligament width and interligament gap increases, whereas on increasing the annealing time from 1 to 3 h, the structure starts to fuse at certain regions forming flat structure whereas at the other regions thinner ligaments start to form due to diffusion of gold

atoms away from that region. Figure 2.10 shows the cross-section images of the np-Au

prepared in the corresponding conditions as Figure 2.9. The cross-section images show the

cracks created during the sample preparation and in general, the ligament width and

interligament gaps of the interior were found to be slightly larger than the exterior as can be

seen from histogram of Figure 2.11. The interior of the np-Au, however, show smaller fusing

effect compared to exterior at both higher dealloying and annealing time. A similar trend has

been found for 0.25 mm thick np-Au plate shown in Figures 2.12, 2.13 and 2.14.
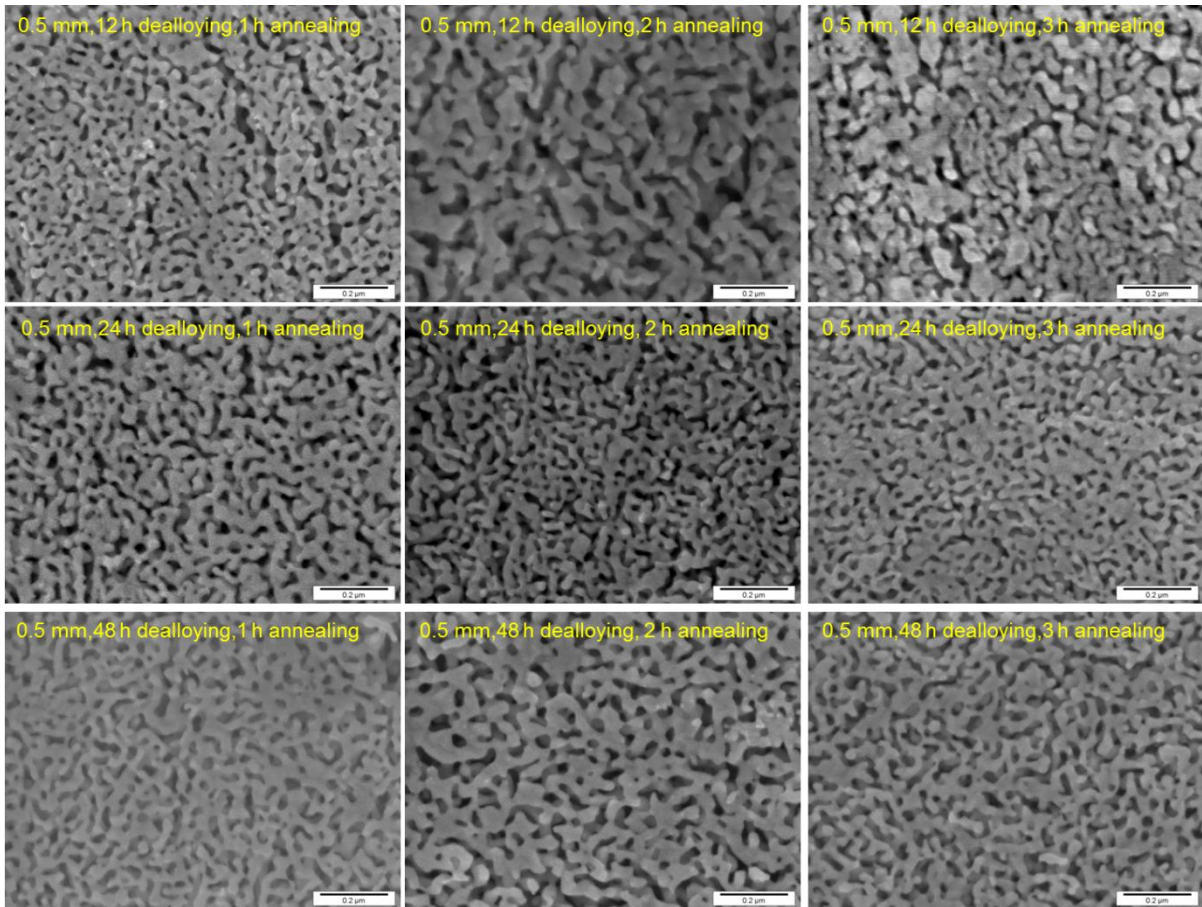
Figure 2.9 SEM images of exterior morphology of the np-Au of 0.5 mm thick plate, dealloyed for different times. First row, 12 h dealloying; second row, 24 h dealloying; and third row, 48 h dealloying and annealing for different time: first column, 1 h; second column, 2 h; and third column, 3 h. All scale bars = 0.2μm.
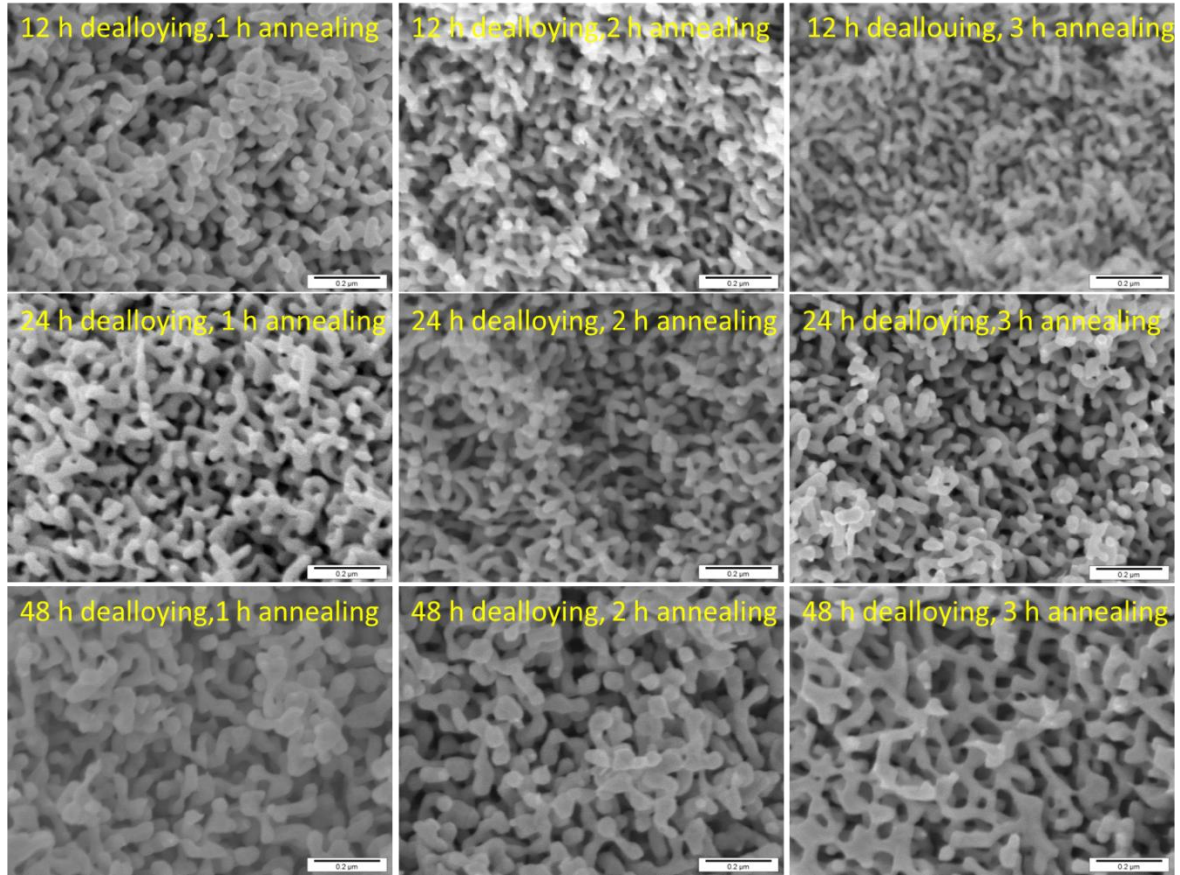
Figure 2.10 SEM micrographs of cross section of 0.5 mm thick np-Au, prepared by dealloying for different time periods: first row, 12 h; second row, 24 h; and third row, 48 h followed by annealing for different time periods: first column, 1 h; second column, 2 h; and third column, 3 h. All scale bars = 0.2μm.
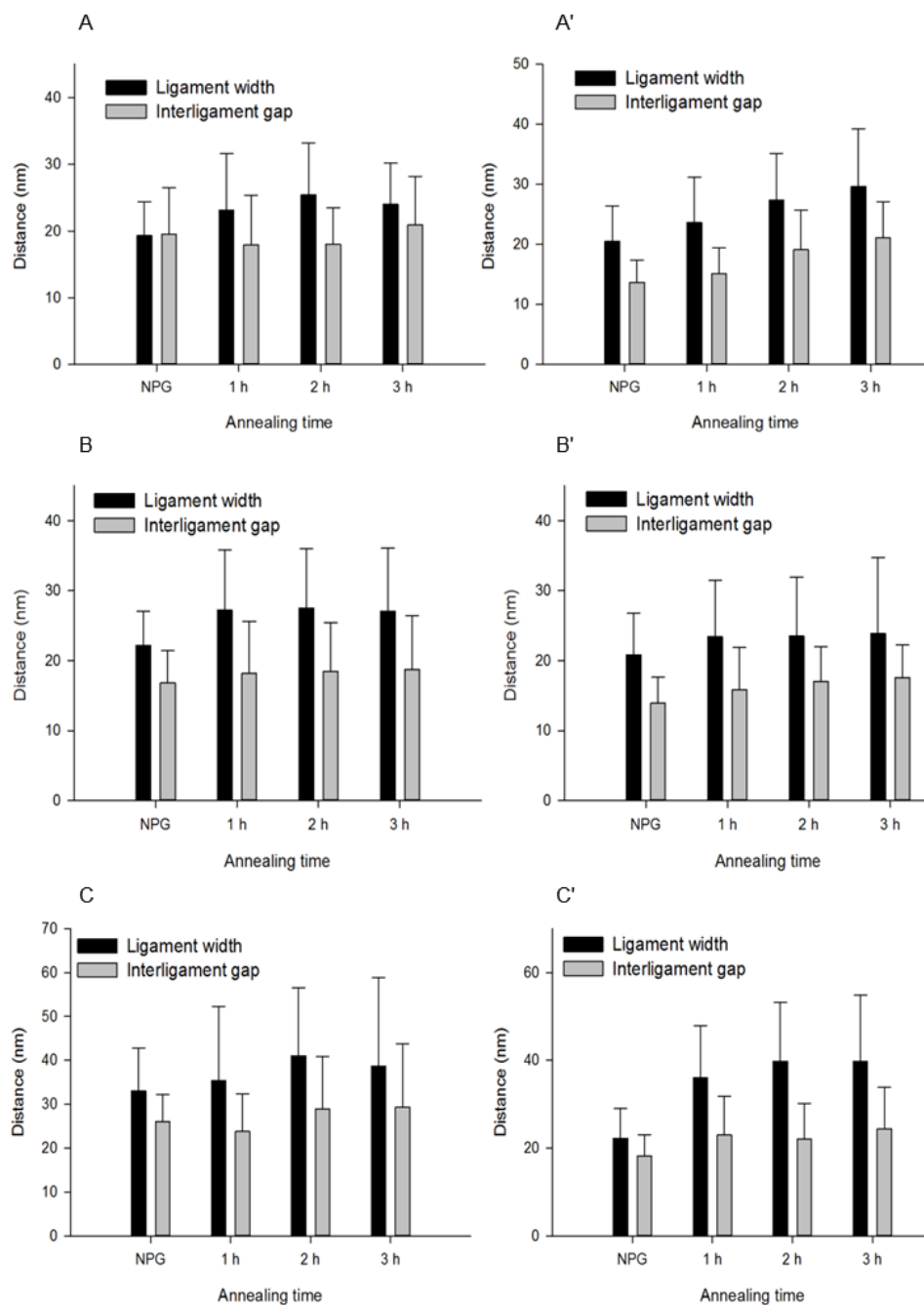
Figure 2.11. Histograms showing change in ligament width and interligament gaps of 0.5 mm thick np-Au prepared by dealloying for 12 h (A, A'), 24 h (B, B') and 48 h (C, C') after annealing at 300 ℃ for different times (1 h, 2 h, and 3 h). A, B and C: interior analysis; A', B' and C': exterior analysis.
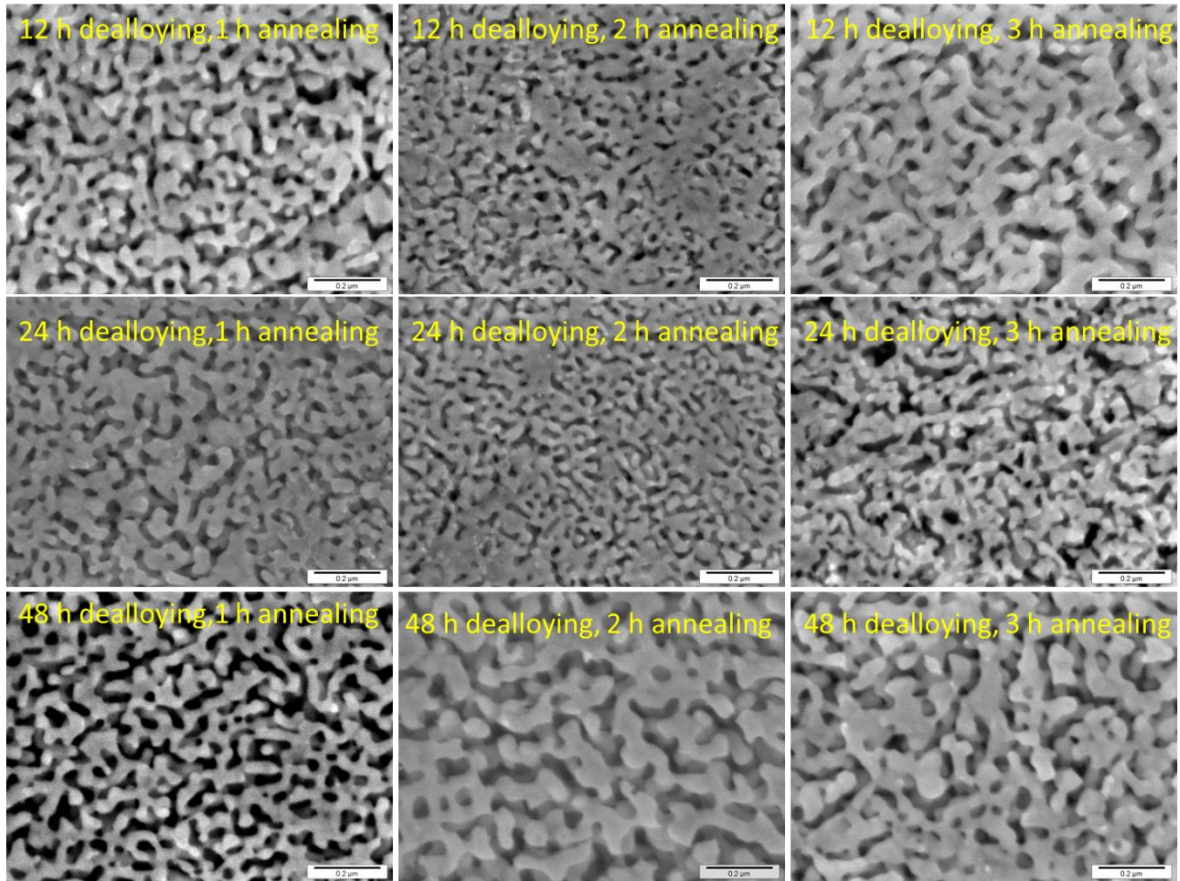
Figure 2.12 SEM of exterior of the np-Au of 0.25 mm thick, dealloying in different times: first row 12 h dealloying, second row 24 h dealloying, and third row 48 h dealloying and annealing in different times: first column, 1 h annealing; second column, 2 h annealing; and third column, 3 h annealing. All scale bars = 0.2μm.
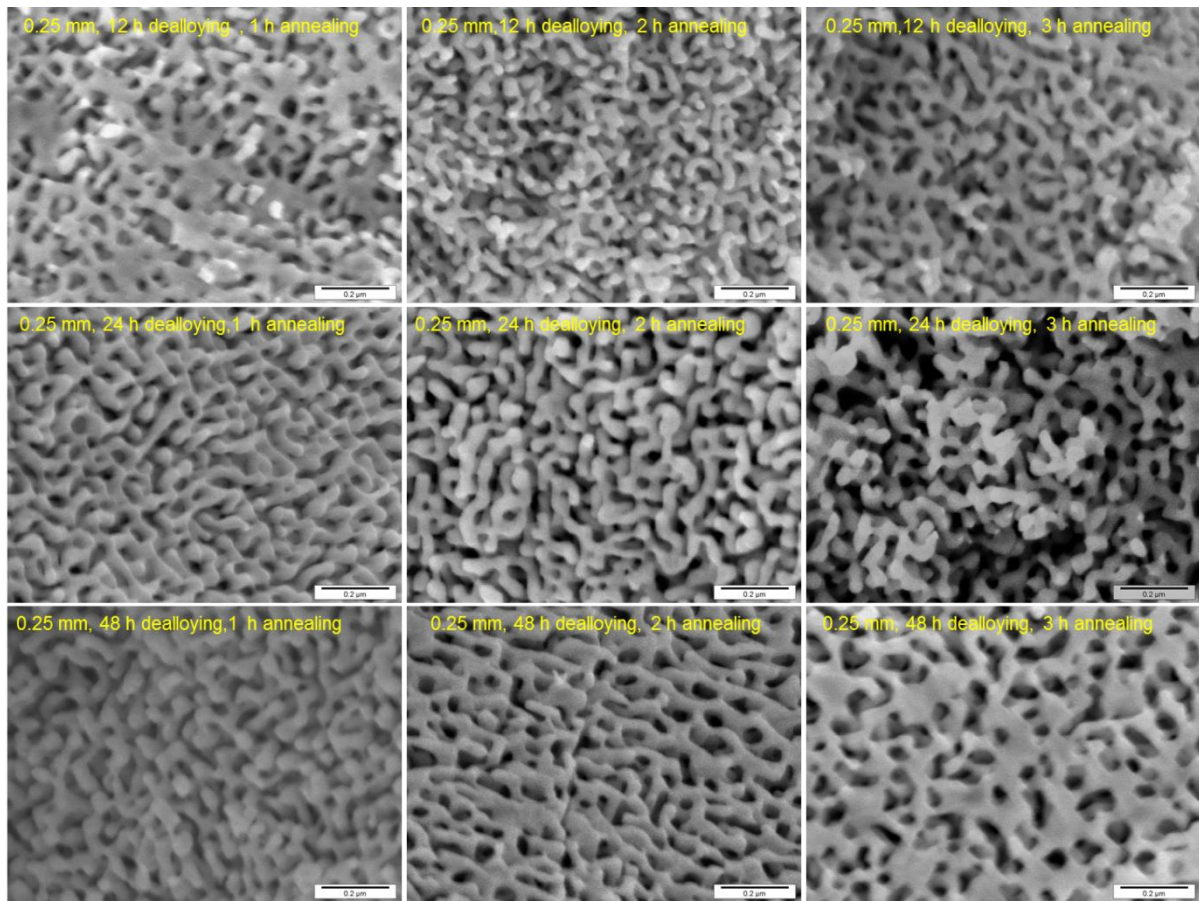
Figure 2.13 SEM of interior of the np-Au of 0.25 mm thick, dealloying in different times; first row, 12 h dealloying; second row, 24 h dealloying; and third row, 48 h dealloying and annealing in different times: first column, 1 h annealing; second column, 2 h annealing; and third column, 3 h annealing. All scale bars = 0.2μm.
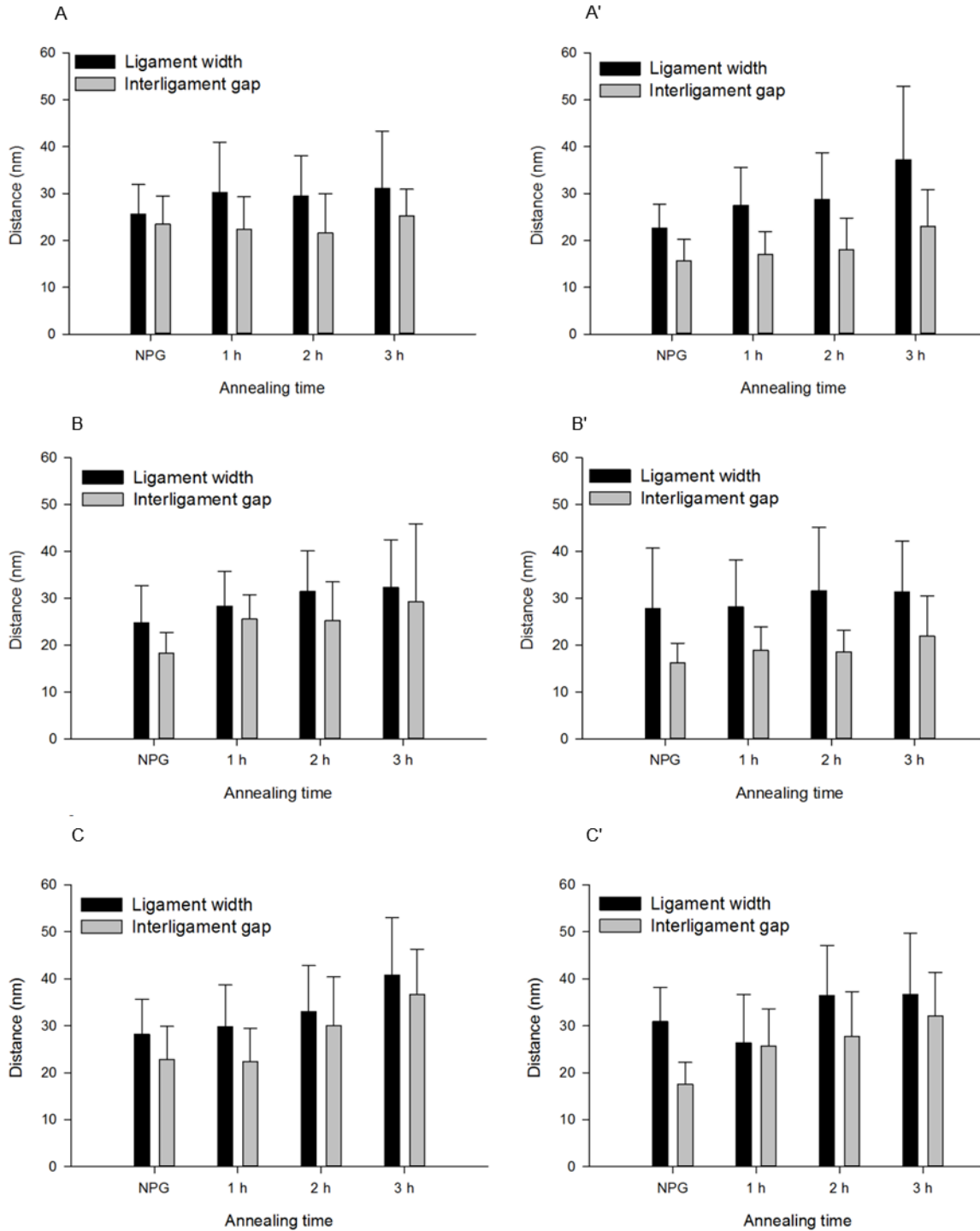
Figure 2. 14 Histograms showing change in ligament width and interligament gaps of 0.25 mm thick np-Au prepared by dealloying for 12 h (A, A'), 24 h (B, B') and 48 h (C, C') after annealing at 300°C for different time (1 h, 2 h, and 3 h). A, B and C: interior analysis; A', B' and C': exterior analysis.

The changes in ligament width and interligament gaps are more obvious in thin gold leaf through SEM images as seen in Figure 2.15. When dealloying time is 48 h and annealing time is 1 h or more at 300°C, only single layer of film can be seen. If the dealloyed time is 12 h or 24 h, single layer of np-Au can be seen within 2 h of annealing. It is also very obvious that with increase in dealloying and annealing time, ligament width and interligament gaps increases drastically. Figure 2.16 shows the ImageJ based analysis of ligament width and interligament gaps.
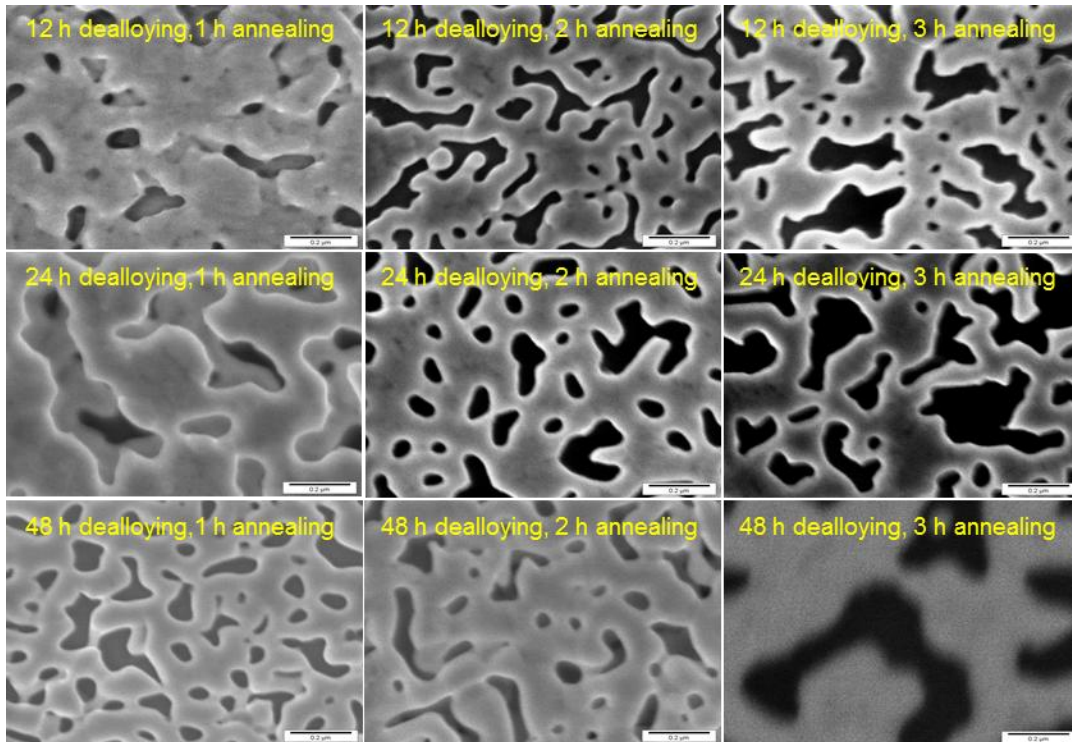
Figure 2.15 SEM of exterior of the np-Au of 200 nm thick, dealloying in different times: first row, 12 h dealloying; second row, 24 h dealloying; and third row, 48 h dealloying and annealing in different times: first column, 1 h annealing; second column, 2 h annealing;, and third column, 3 h annealing. All scale bars = 0.2μm.
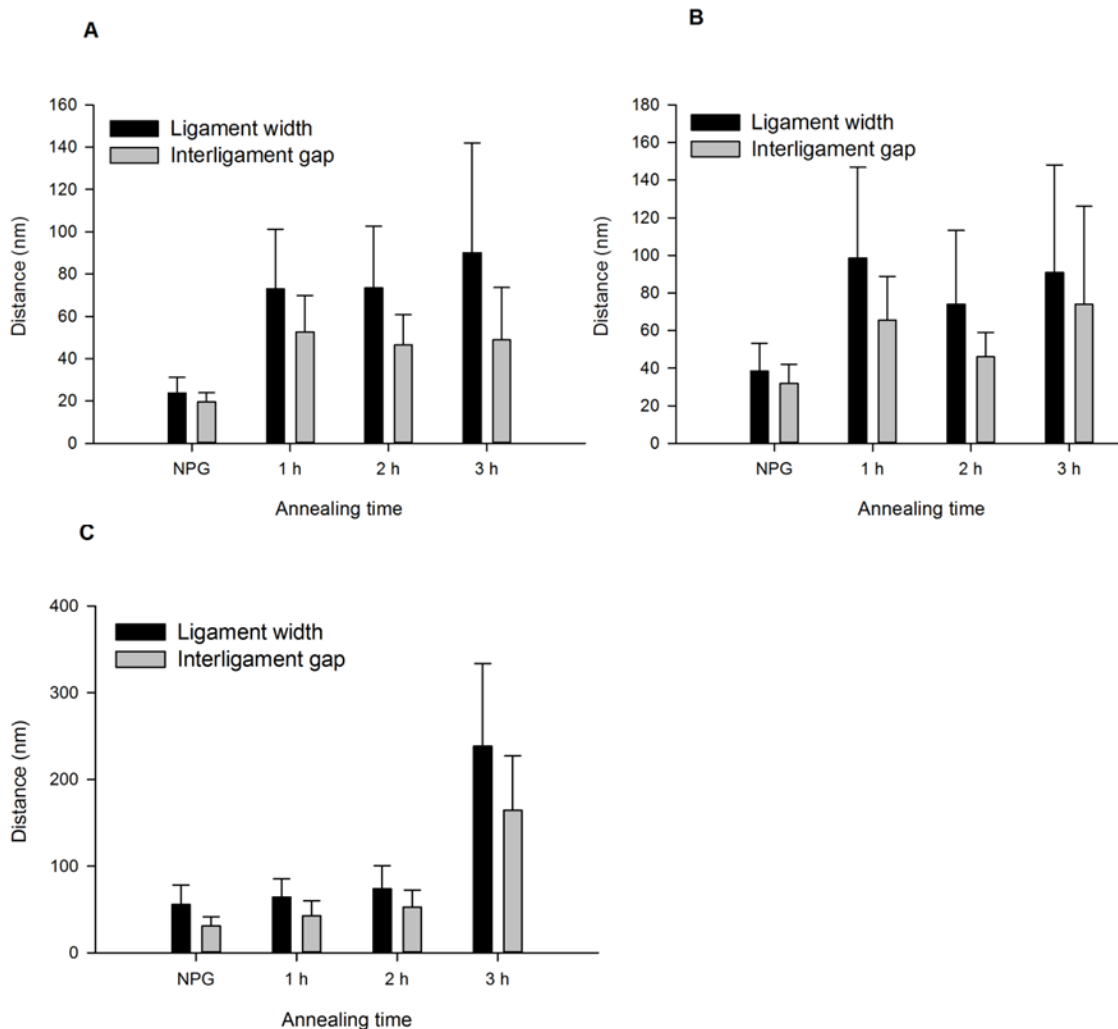
Figure 2.16 Histograms showing change in ligament width and interligament gaps at 300°C on increasing time of 200 nm thick. A: 12 h dealloying, B: 24 h dealloying and C: 48 h dealloying.

2.3 Conclusions

Both the amount of time and the strength of the dealloying solution are significant factors in the preparation of np-Au. In the dealloying process, the results show that excess volume of nitric acid is critical for the removal of less noble metals. By providing the excess volume, the dealloying time can be drastically decreased while properly removing the less noble metals. It was concluded that 5 mL nitric acid per plate condition is optimal for

removal of less noble metal from gold to prepare np-Au. Both dealloying time and annealing time have strong effects on ligament width and interligament gaps. These increase dramatically by longer exposure. The ligament width and interligament gaps of np-Au monoliths can be readily tuned by thermal annealing. Study of np-Au annealed at 200, 300, and 400°C has found that annealing produces significant changes in film thickness and average pore size. At 300°C, clearly distinguishable Au clusters are formed and the pore size increases dramatically. The interior of the np-Au, however, show smaller fusing effect compared to exterior at both higher dealloying and annealing time. With an increase in dealloying time, the ligament width and interligament gap increases. Increasing the annealing time from 1 to 3 hours causes structural issues. The structure starts to fuse at certain regions forming flat structures whereas at the other regions thinner ligaments start to form due to diffusion away of gold atoms from that region.

The differences in morphology of np-Au plates having thickness very close to 0.25 mm versus 0.50 were not obvious, but when compared to the thinner np-Au leaf (200 nm) the ligament widths and interligament gaps change drastically.

Chapter 3   Study of the Fluorescein Release from Modified np-Au

3.1 Experimental Methods

3.1.1 Electroless deposition of gold/silver alloy on np-Au

The autocatalytic electroless plating on np-Au was done by using the recipe of Okinaka,[79] which uses $KAu(CN)_2$ as gold precursor, $KAg(CN)_2$ as silver precursor, NaCN to improve the ductility of the deposit, KOH to make the plating solution strongly basic, and $NaBH_4$ as the reducing agent. The composition of the mixture for electroless deposition was prepared following the table below and diluted by the factor of ten.[79]

Table 3-1 Components of electroless plating bath.

Components	Concentrations(M)	Molar Mass (g/mol)	Mass(mg)
$KAu(CN)_2$	0.026	288.11	187
$KAg(CN)_2$	0.007	199.01	34.8
NaCN	0.010	49.01	12.3
KOH	0.200	56.11	280.6
$NaBH_4$	0.200	37.80	189.2

After dealloying 48 h and annealing for 2 h at 300 °C, electroless deposition was used to deposite a 0.25 mm thick layer. Electroless deposition was performed at 80°C for 1 min and 5 min, rinsed the pieces 3 times with Mill-Q water and then by ethanol. After drying the pieces, they are placed in HNO_3 for 30 min to remove silver selectively from the gold. The

plates were then rinsed three times with Mill-Q water and then by ethanol. They are kept in vacuum until further used for loading fluorescein or characterizing.

3.1.2 Loading of fluorescein on np-Au and modified np-Au monolith

Nanoporous gold monoliths with or without modification were loaded with a 50 µL fluorescein sodium salt solution (concentration of 10 mM in 50 mL) either in a static or flow condition. In a static method, fluorescein was incubated for 16 hours inside a 50 µL fluorescein sodium salt solution in a microcentrifuge tube at room temperature without exposure to light by wrapping with foil. In the flow method, a peristaltic pump is used to load the fluorescein inside the monoliths placed in the flow cell. The rate of flow was maintained at 0.2 ml /min and 5 ml of fluorcescein sodium salt solution was cycled through the flow cell for 30 min. The fluorescein-loaded plates were then rinsed three times with Milli-Q water for 10 s in order to wash off any residual fluorescein molecules from the outside surface of the samples.

3.1.3 UV-Vis monitoring of fluorescein release

The release of fluorescein molecules from nanoporous gold monolith into the buffer solution was monitored using UV-Vis spectrophotometer (Cary 500), which measures the absorbance of the solution at wavelength of 515 nm.

3.2 Results and Discussion

3.2.1 Electroless deposition of gold/silver alloy on np-Au

Figure 3.1 shows home-built set up for electroless deposition of gold/silver alloy on np-Au. It consists of water bath placed on top of a heating plate and borohydride bath in

microcentrifuge tube, which is held by a Teflon cover in one end and dipped in a water bath at the other end. A thermometer is dipped into the water bath to record the temperature. The np-Au plate is immersed into the borohydride bath for the electroless deposition and temperature is maintained to accelerate the reaction.
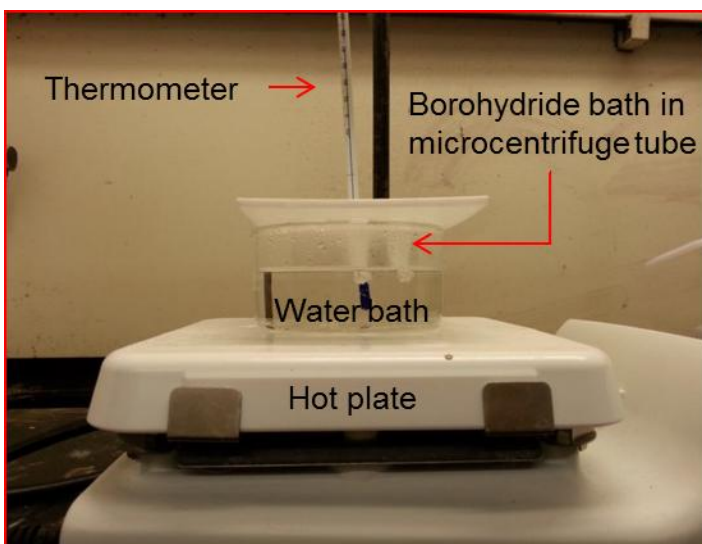
Figure 3.1 Set-up of electroless plating

For the use of np-Au as a substrate to hold a large amount of drug and release in control or slow speed, it should have a large surface area inside but with the smaller openings. Np-Au within itself can hold a large amount of drug molecules but its release to the local environment is faster. Here, we tried to modify the opening of np-Au surface without disturbing the interior structure of the np-Au.

Figure 3.2 A shows SEM image of np-Au monolith after 5 min of electroless deposition of gold and silver alloy. It can be seen that within five minutes of electroless deposition all the pores and ligaments of np-Au are covered with the alloy of gold/silver. Figure 3.2 A is a cross section image of the same np-Au showing all the pore and ligament of

np-Au. Figure 3.2 B is the SEM image after the dealloying of the electroless deposit for 24 hours in nitric acid. It can be seen that the covered surface is almost all open due to a longer period of dealloying of the thin deposit forming the randomly fused structure. We have discussed this type of effect in previous chapter. We have also seen some modification on initial pores of np-Au monolith, which should be due to combination of different effects, such as 24 hour of added dealloying time, heat used in electroless deposition and deposited alloy. As before, we can still see the ligaments and pores in the cross section but with the increase in both ligament width and interligament gaps, which should be because of added dealloying time. Therefore, dealloying time was decreased to 30 min to reduce the diffusing effect of deposited and dealloyed gold structure.
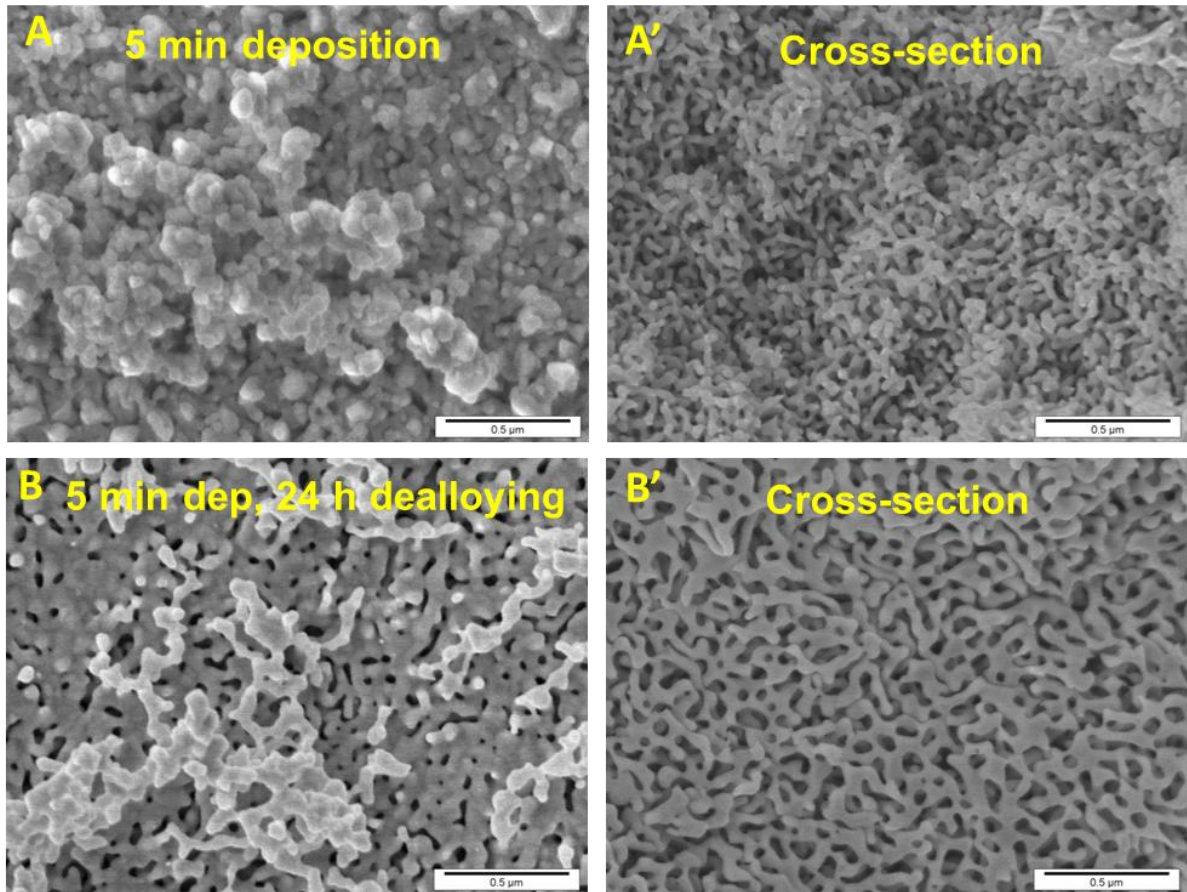
Figure 3.2 SEM image of np-Au plate after 5 min of electroless deposition of alloy. All scale bars =0.5μm.

Figure 3.3 shows the SEM images of np-Au after 1 and 5 min alloy deposition and dealloyed for 30 min. The corresponding cross-section images are also shown. It can be seen that 5min deposition and 30 min dealloyed structure does not have fully visible ligament and pores but still some pores can be seen. However, 1 min deposition and 30 min dealloyed np-Au monolith have clearly visible pores and ligaments. On the other hand, the interior structures of both look similar. These 1 and 5 min electroless deposited and 30 min dealloyed

np-Au monolith are the desired structure to load the drug, so their drug releasing time, using

fluorescein as a model, is compared with that of unmodified np-Au.
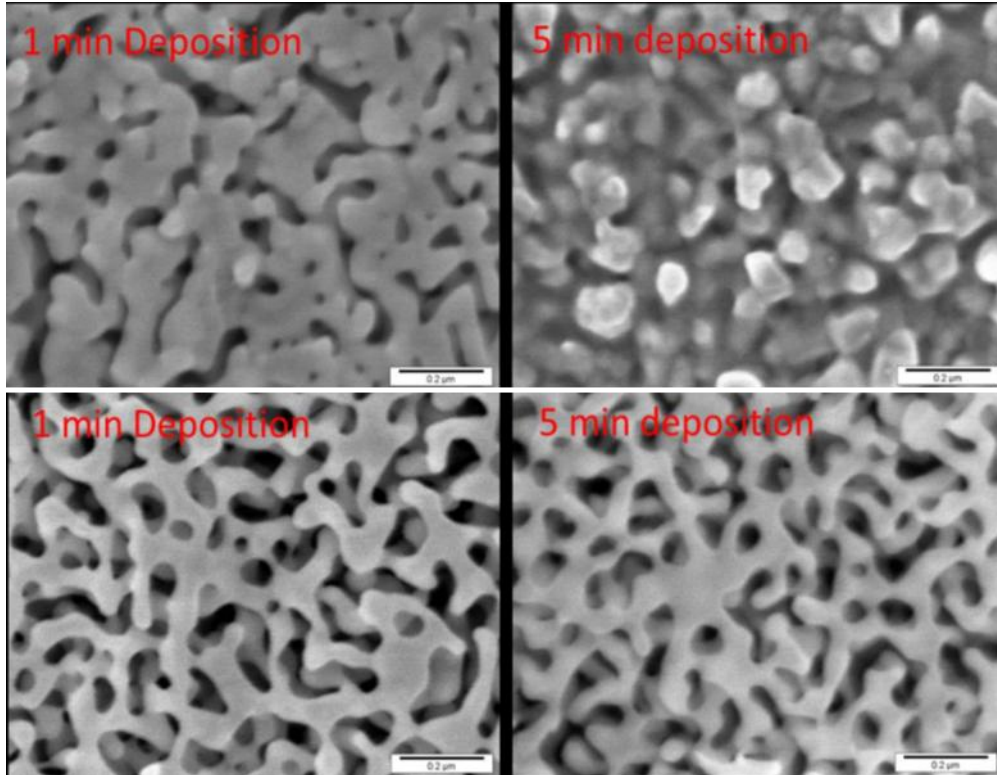
Figure 3.3 SEM images of modified np-Au prepared at **left two:** 1 min deposition at 80°C + dealloying 30 min and **right two:** 5 min deposition at 80°C + dealloying 30 min. Upper panel: exterior and lower panel: interior. All scale bars = 0.2µm.

3.2.2   Fluorescein loading and quantification

Fluorescein is loaded in the np-Au and modified np-Au mainly through two

processes–static and flow through. In the static process the np-Au and modified np-Au is

simply immersed in the fluorescein solution, whereas in the flow through method, a

peristaltic pump is used to force the fluorescein solution to pass through the structures. The

set-up of the flow through process is shown in Figure 3.4.
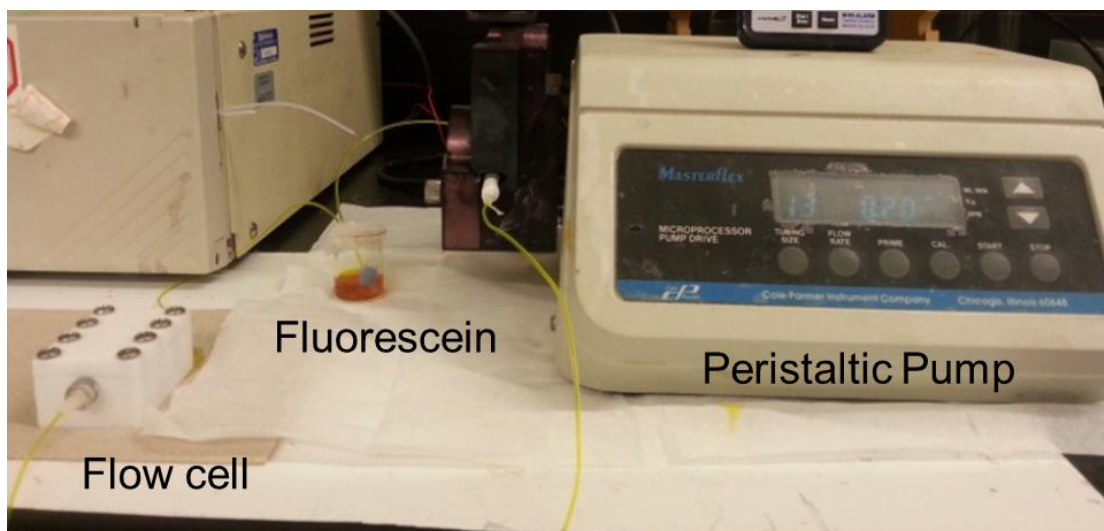
Figure 3.4 Set-up for flowing fluorescein through the np-Au structures placed in flow cell.

3.2.3 Study of the release of fluorescein from np-Au

Due to its unique characteristics, nanoporous gold has great potential to be used as a delivery mechanism for molecules. Recently, Polata and Seker examined the release of fluorescein molecules (a small-molecule drug surrogate) from np-Au.[86-87] They studied the loading capacity and releasing kinetics of np-Au structures due to halide ions interfacial interactions and self-assembled monolayer prepared on the surface of np-Au.

Here, we are performing similar work but controlling the opening of np-Au by electroless deposition of gold/silver alloy followed by dealloying for loading and time dependent release of the fluorescein. The release profile of np-Au monolith with or without modification was monitored by sampling the buffer media at specific time points followed by quantifying its fluorescein intensity (emission at $\lambda = 515$ nm) with UV-Vis spectrophotometer. The buffer media is made up of 2.67 mM KCl, 1.47 mM potassium phosphate monobasic (H_2KD_4P), 8.06 mM sodium phosphate dibasic (Na_2HPO_4), and 136.9 mM sodium chloride (NaCl) by dissolving in 500 ml Milli-Q water. Nanoporous gold

monolith loaded with fluorescein was placed in 300 μL of buffer media in the cuvette for

UV-Vis reading. The UV–Vis spectrometer and the computer connected to it is shown in

Figure 3.5.

Figure 3.5 UV-Vis spectrophotometer and connected computer used to study the fluorescein release from np-Au

Fluorescein molecules can absorb light in the visible region. Initially, the phosphate

buffer saline shows zero absorbance. With the release of fluorescein from np-Au to the buffer

solution, the absorbance of light due to the solution starts increasing. Figure 3.7 show the

release of fluorescein to the buffer from static and flow loaded samples. In the static method,

it can be seen that fluorescein release is faster through the np-Au compared to through the

modified np-Au. However, the intensity of the absorbance was found to be saturated within

20 min for all the samples, which also means that in the modified np-Au not enough

fluorescein was loaded because of smaller pore size on the surface. However, when the flow

method was used to load the fluorescein, the absorbance saturates at 0.2805 absorption unit

for np-Au, which is twice compared to the static method. However, the fluorescein-releasing

rate is faster and saturation is reached quickly. 1 and 5 min alloy deposited np-Au shows the

slow release of the molecule evident by increasing absorbance within 30 min. It is clear from these experiments that modification of np-Au by electroless deposition of Au/Ag alloy followed by 30 min dealloying and flow-based loading are important factors for the improvement of the drug release system using np-Au substrate.
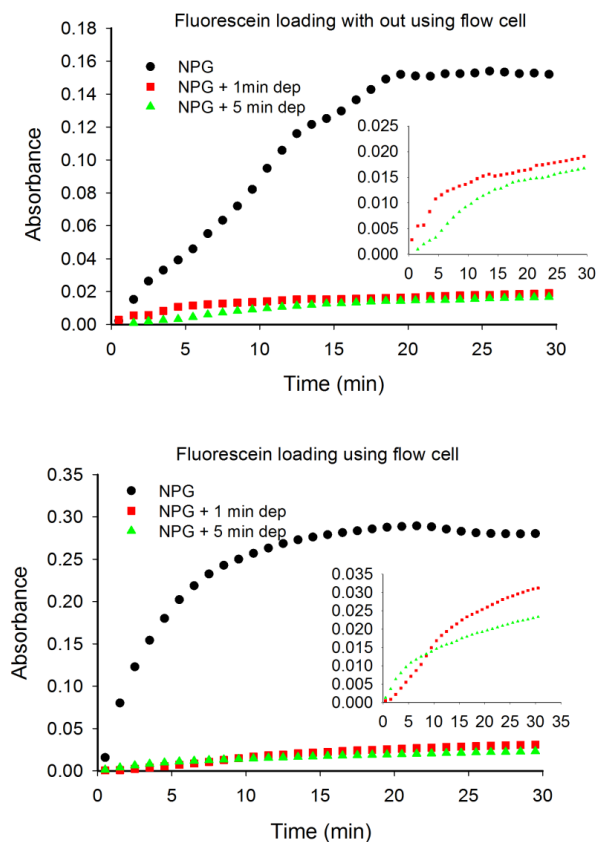
Figure 3.6 Plots showing the release of fluorescein from np-Au with increase in time. The top image is when fluorescein was loaded in static condition, and bottom is when fluorescein was loaded using flow cell.

3.3 Conclusions

In the static method, the fluorescein release is faster through the np-Au compared to through the modified np-Au. However, the intensity of the absorbance was found to be

saturated within 20 min for all the samples, which also means that in the modified np-Au not enough fluorescein was loaded because of smaller pore size on the surface.

However, when the flow method was used to load the fluorescein, the absorbance saturates at 0.2805 absorption unit for np-Au, which is twice as much compared to the static method. However, the fluorescein-releasing rate is faster and saturation is reached quickly. It is clear from these experiments that modification of np-Au by electroless deposition of Au/Ag alloy followed by 30 min dealloying and flow-based loading are important factors for the improvement of the drug release system using np-Au substrate.

References

1. Sun, I.-W.; Chen, P.-Y., Nanoporous Gold in Sensor Applications. In *Nanoporous Gold*, 2012; pp 224-247.

2. Ahn, S.; Lee, J.; Kim, H.; Kim, J., A Study on the Quantitative Determination of through-Coating Porosity in Pvd-Grown Coatings. *Applied Surface Science* **2004,** *233* (1), 105-114.

3. Li, C.; Dag, Ö.; Dao, T. D.; Nagao, T.; Sakamoto, Y.; Kimura, T.; Terasaki, O.; Yamauchi, Y., Electrochemical Synthesis of Mesoporous Gold Films toward Mesospace-Stimulated Optical Properties. *Nature communications* **2015,** *6*.

4. Ding, C.; Li, H.; Hu, K.; Lin, J.-M., Electrochemical Immunoassay of Hepatitis B Surface Antigen by the Amplification of Gold Nanoparticles Based on the Nanoporous Gold Electrode. *Talanta* **2010,** *80* (3), 1385-1391.

5. Shulga, O. V.; Zhou, D.; Demchenko, A. V.; Stine, K. J., Detection of Free Prostate Specific Antigen (Fpsa) on a Nanoporous Gold Platform. *Analyst* **2008,** *133* (3), 319-322.

6. Zhu, A.; Tian, Y.; Liu, H.; Luo, Y., Nanoporous Gold Film Encapsulating Cytochrome C for the Fabrication of a H 2 O 2 Biosensor. *Biomaterials* **2009,** *30* (18), 3183-3188.

7. Tan, Y. H.; Schallom, J. R.; Ganesh, N. V.; Fujikawa, K.; Demchenko, A. V.; Stine, K. J., Characterization of Protein Immobilization on Nanoporous Gold Using Atomic Force Microscopy and Scanning Electron Microscopy. *Nanoscale* **2011,** *3* (8), 3395-3407.

8. Pandey, B.; Tan, Y. H.; Fujikawa, K.; Demchenko, A. V.; Stine, K. J., Comparative Study of the Binding of Concanavalin a to Self-Assembled Monolayers Containing a Thiolated A-Mannoside on Flat Gold and on Nanoporous Gold. *Journal of carbohydrate chemistry* **2012,** *31* (4-6), 466-503.

9. Ju, H., Sensitive Biosensing Strategy Based on Functional Nanomaterials. *Science China Chemistry* **2011,** *54* (8), 1202-1217.

10. Yu, F.; Ahl, S.; Caminade, A.-M.; Majoral, J.-P.; Knoll, W.; Erlebacher, J., Simultaneous Excitation of Propagating and Localized Surface Plasmon Resonance in Nanoporous Gold Membranes. *Analytical chemistry* **2006,** *78* (20), 7346-7350.

11. Bok, H.-M.; Shuford, K. L.; Kim, S.; Kim, S. K.; Park, S., Multiple Surface Plasmon Modes for a Colloidal Solution of Nanoporous Gold Nanorods and Their Comparison to Smooth Gold Nanorods. *Nano letters* **2008,** *8* (8), 2265-2270.

12. Ji, C.; Searson, P. C., Synthesis and Characterization of Nanoporous Gold Nanowires. *The Journal of Physical Chemistry B* **2003,** *107* (19), 4494-4499.

13. Wittstock, A.; Zielasek, V.; Biener, J.; Friend, C.; Bäumer, M., Nanoporous Gold Catalysts for Selective Gas-Phase Oxidative Coupling of Methanol at Low Temperature. *Science* **2010,** *327* (5963), 319-322.

14. Xu, C.; Su, J.; Xu, X.; Liu, P.; Zhao, H.; Tian, F.; Ding, Y., Low Temperature Co Oxidation over Unsupported Nanoporous Gold. *Journal of the American Chemical Society* **2007,** *129* (1), 42-43.

15. Jiang, J.; Li, Y.; Liu, J.; Huang, X.; Yuan, C.; Lou, X. W. D., Recent Advances in Metal Oxide‐ Based Electrode Architecture Design for Electrochemical Energy Storage. *Advanced materials* **2012,** *24* (38), 5166-5180.

16. Ding, Y.; Kim, Y. J.; Erlebacher, J., Nanoporous Gold Leaf:"Ancient Technology"/Advanced Material. *Advanced Materials* **2004,** *16* (21), 1897-1900.

17. Whitesides, G. M.; Mathias, J. P.; Seto, C. T. *Molecular Self-Assembly and Nanochemistry: A Chemical Strategy for the Synthesis of Nanostructures*; DTIC Document: 1991.

18. Pokropivny, V.; Skorokhod, V., Classification of Nanostructures by Dimensionality and Concept of Surface Forms Engineering in Nanomaterial Science. *Materials Science and Engineering: C* **2007,** *27* (5), 990-993.

19.   Bhattarai, J. K. Electrochemical Synthesis of Nanostructured Noble Metal Films for Biosensing. University of Missouri-St. Louis, **2014**.

20.   Zhang, L.; Lang, X.; Hirata, A.; Chen, M., Wrinkled Nanoporous Gold Films with Ultrahigh Surface-Enhanced Raman Scattering Enhancement. *ACS nano* **2011,** *5* (6), 4407-4413.

21.   Lefebvre, L.-P.; Banhart, J.; Dunand, D., Porous Metals and Metallic Foams: Current Status and Recent Developments. *Advanced Engineering Materials* **2008,** *10* (September 9), 775-787.

22.   Kim, M.-S.; Nishikawa, H., Fabrication of Nanoporous Silver and Microstructural Change During Dealloying of Melt-Spun Al–20 at.%Ag in Hydrochloric Acid. *Journal of Materials Science* **2013,** *48* (16), 5645-5652.

23.   Qi, Z.; Zhao, C.; Wang, X.; Lin, J.; Shao, W.; Zhang, Z.; Bian, X., Formation and Characterization of Monolithic Nanoporous Copper by Chemical Dealloying of Al− Cu Alloys. *The Journal of Physical Chemistry C* **2009,** *113* (16), 6694-6698.

24.   Liu, W.; Zhang, S.; Li, N.; Zheng, J.; Xing, Y., Influence of Phase Constituent and Proportion in Initial Al–Cu Alloys on Formation of Monolithic Nanoporous Copper through Chemical Dealloying in an Alkaline Solution. *Corrosion Science* **2011,** *53* (2), 809-814.

25.   Dan, Z.; Qin, F.; Sugawara, Y.; Muto, I.; Hara, N., Fabrication of Nanoporous Copper by Dealloying Amorphous Binary Ti–Cu Alloys in Hydrofluoric Acid Solutions. *Intermetallics* **2012,** *29*, 14-20.

26.   Liu, W.; Zhang, S.; Li, N.; An, S.; Zheng, J., Formation of Monolithic Nanoporous Copper with Ultrahigh Specific Surface Area through Chemical Dealloying of Mg-Cu Alloy. *Int. J. Electrochem. Sci.* **2012,** *7*, 9707-9716.

27.   Chamoun, M.; Hertzberg, B. J.; Gupta, T.; Davies, D.; Bhadra, S.; Van Tassell, B.; Erdonmez, C.; Steingart, D. A., Hyper-Dendritic Nanoporous Zinc Foam Anodes. *NPG Asia Materials* **2015,** *7* (4), e178.

28.   Adkins, H.; Billica, H. R., The Preparation of Raney Nickel Catalysts and Their Use under Conditions Comparable with Those for Platinum and Palladium Catalysts. *Journal of the American Chemical Society* **1948,** *70* (2), 695-698.

29.   Hodge, A. M.; Hayes, J. R.; Caro, J. A.; Biener, J.; Hamza, A. V., Characterization and Mechanical Behavior of Nanoporous Gold. *Advanced Engineering Materials* **2006,** *8* (9), 853-857.

30.   Erlebacher, J.; Aziz, M. J.; Karma, A.; Dimitrov, N.; Sieradzki, K., Evolution of Nanoporosity in Dealloying. *Nature* **2001,** *410* (6827), 450-453.

31.   Detsi, E.; Van De Schootbrugge, M.; Punzhin, S.; Onck, P.; De Hosson, J., On Tuning the Morphology of Nanoporous Gold. *Scripta Materialia* **2011,** *64* (4), 319-322.

32.   Okman, O., Nanoporous Gold: Mechanics of Fabrication and Actuation. **2012**.

33.   Snyder, J.; Asanithi, P.; Dalton, A. B.; Erlebacher, J., Stabilized Nanoporous Metals by Dealloying Ternary Alloy Precursors. *Advanced Materials* **2008,** *20* (24), 4883-4886.

34.   Huang, J. F.; Sun, I. W., Fabrication and Surface Functionalization of Nanoporous Gold by Electrochemical Alloying/Dealloying of Au–Zn in an Ionic Liquid, and the Self- Assembly of L- Cysteine Monolayers. *Advanced Functional Materials* **2005,** *15* (6), 989-994.

35.   Qian, L.; Chen, M., Ultrafine Nanoporous Gold by Low-Temperature Dealloying and Kinetics of Nanopore Formation. *Applied Physics Letters* **2007,** *91* (8), 083105.

36.   Detsi, E.; Punzhin, S.; Rao, J.; Onck, P. R.; De Hosson, J. T. M., Enhanced Strain in Functional Nanoporous Gold with a Dual Microscopic Length Scale Structure. *Acs Nano* **2012,** *6* (5), 3734-3744.

37.   Kertis, F.; Snyder, J.; Govada, L.; Khurshid, S.; Chayen, N.; Erlebacher, J., Structure/Processing Relationships in the Fabrication of Nanoporous Gold. *Jom* **2010,** *62* (6), 50-56.

38.   Sharma, A.; Bhattarai, J. K.; Alla, A. J.; Demchenko, A. V.; Stine, K. J., Electrochemical Annealing of Nanoporous Gold by Application of Cyclic Potential Sweeps. *Nanotechnology* **2015,** *26* (8), 085602.

39.   Detsi, E.; De Jong, E.; Zinchenko, A.; Vuković, Z.; Vuković, I.; Punzhin, S.; Loos, K.; Ten Brinke, G.; De Raedt, H.; Onck, P., On the Specific Surface Area of Nanoporous Materials. *Acta Materialia* **2011,** *59* (20), 7488-7497.

40.   Tan, Y. H.; Davis, J. A.; Fujikawa, K.; Ganesh, N. V.; Demchenko, A. V.; Stine, K. J., Surface Area and Pore Size Characteristics of Nanoporous Gold Subjected to Thermal, Mechanical, or Surface Modification Studied Using Gas Adsorption Isotherms, Cyclic Voltammetry, Thermogravimetric Analysis, and Scanning Electron Microscopy. *Journal of materials chemistry* **2012,** *22* (14), 6733-6745.

41.   Von Blanckenhagen, P.; Göbel, H., A Low Temperature Leed Study of the Au (110) Surface. *surface science* **1995,** *331*, 1082-1084.

42.   Seker, E.; Gaskins, J. T.; Bart-Smith, H.; Zhu, J.; Reed, M. L.; Zangari, G.; Kelly, R.; Begley, M. R., The Effects of Post-Fabrication Annealing on the Mechanical Properties of Freestanding Nanoporous Gold Structures. *Acta Materialia* **2007,** *55* (14), 4593-4602.

43.   Biener, J.; Wittstock, A.; Zepeda-Ruiz, L.; Biener, M.; Zielasek, V.; Kramer, D.; Viswanath, R.; Weissmüller, J.; Bäumer, M.; Hamza, A., Surface-Chemistry-Driven Actuation in Nanoporous Gold. *Nature materials* **2009,** *8* (1), 47-51.

44.   Biener, J.; Nyce, G. W.; Hodge, A. M.; Biener, M. M.; Hamza, A. V.; Maier, S. A., Nanoporous Plasmonic Metamaterials. *Advanced Materials* **2008,** *20* (6), 1211-1217.

45.   Ahn, W.; Roper, D. K., Periodic Nanotemplating by Selective Deposition of Electroless Gold Island Films on Particle-Lithographed Dimethyldichlorosilane Layers. *ACS nano* **2010,** *4* (7), 4181-4189.

46.   Mansfield, E.; Tyner, K. M.; Poling, C. M.; Blacklock, J. L., Determination of Nanoparticle Surface Coatings and Nanoparticle Purity Using Microscale Thermogravimetric Analysis. *Analytical chemistry* **2014,** *86* (3), 1478-1484.

47.   Tappan, B. C.; Steiner, S. A.; Luther, E. P., Nanoporous Metal Foams. *Angewandte Chemie International Edition* **2010,** *49* (27), 4544-4565.

48.   Gelb, L. D.; Gubbins, K., Characterization of Porous Glasses: Simulation Models, Adsorption Isotherms, and the Brunauer-Emmett-Teller Analysis Method. *Langmuir* **1998,** *14* (8), 2097-2111.

49.   Joyner, L. G.; Barrett, E. P.; Skold, R., The Determination of Pore Volume and Area Distributions in Porous Substances. Ii. Comparison between Nitrogen Isotherm and Mercury Porosimeter Methods. *Journal of the American Chemical Society* **1951,** *73* (7), 3155-3158.

50.   Vesel, A.; Junkar, I.; Cvelbar, U.; Kovac, J.; Mozetic, M., Surface Modification of Polyester by Oxygen‐ and Nitrogen‐ Plasma Treatment. *Surface and interface analysis* **2008,** *40* (11), 1444-1453.

51.   Gutowski, W. V.; Dodiuk, H., *Recent Advances in Adhesion Science and Technology in Honor of Dr. Kash Mittal*. CRC Press: **2013**.

52.   Ron, H.; Rubinstein, I., Alkanethiol Monolayers on Preoxidized Gold. Encapsulation of Gold Oxide under an Organic Monolayer. *Langmuir* **1994,** *10* (12), 4566-4573.

53.   Hou, X.; Guo, W.; Xia, F.; Nie, F.-Q.; Dong, H.; Tian, Y.; Wen, L.; Wang, L.; Cao, L.; Yang, Y., A Biomimetic Potassium Responsive Nanochannel: G-Quadruplex DNA Conformational Switching in a Synthetic Nanopore. *Journal of the American Chemical Society* **2009,** *131* (22), 7800-7805.

54.   Sebby, K.; Mansfield, E., Determination of the Surface Density of Polyethylene Glycol on Gold Nanoparticles by Use of Microscale Thermogravimetric Analysis. *Analytical and bioanalytical chemistry* **2015,** *407* (10), 2913-2922.

55.   Tan, Y. H.; Fujikawa, K.; Pornsuriyasak, P.; Alla, A. J.; Ganesh, N. V.; Demchenko, A. V.; Stine, K. J., Lectin–Carbohydrate Interactions on Nanoporous Gold Monoliths. *New Journal of Chemistry* **2013,** *37* (7), 2150-2165.

56.   Collinson, M. M., Nanoporous Gold Electrodes and Their Applications in Analytical Chemistry. *ISRN Analytical chemistry* **2013,** *2013*.

57.   Lefebvre, L.-P.; Banhart, J.; Dunand, D., Porous Metals and Metallic Foams: Current Status and Recent Developments. *Advanced Engineering Materials* **2008,** *10* (9), 775-787.

58.   Seker, E.; Reed, M. L.; Begley, M. R., Nanoporous Gold: Fabrication, Characterization, and Applications. *Materials* **2009,** *2* (4), 2188-2215.

59.   Stine, K. J.; Jefferson, K.; Shulga, O. V., Nanoporous Gold for Enzyme Immobilization. *Enzyme Stabilization and Immobilization: Methods and Protocols* **2011**, 67-83.

60.   Weissmüller, J.; Viswanath, R.; Kramer, D.; Zimmer, P.; Würschum, R.; Gleiter, H., Charge-Induced Reversible Strain in a Metal. *Science* **2003,** *300* (5617), 312-315.

61.   Wang, S.; Kristian, N.; Jiang, S.; Wang, X., Controlled Synthesis of Dendritic Au@ Pt Core–Shell Nanomaterials for Use as an Effective Fuel Cell Electrocatalyst. *Nanotechnology* **2008,** *20* (2), 025605.

62.   Yan, X.; Meng, F.; Xie, Y.; Liu, J.; Ding, Y., Direct N2h4/H2o2 Fuel Cells Powered by Nanoporous Gold Leaves. *Scientific reports* **2012,** *2*, 941.

63.   Pornsuriyasak, P.; Ranade, S. C.; Li, A.; Parlato, M. C.; Sims, C. R.; Shulga, O. V.; Stine, K. J.; Demchenko, A. V., Stics: Surface-Tethered Iterative Carbohydrate Synthesis. *Chemical Communications* **2009,** (14), 1834-1836.

64.   Ganesh, N. V.; Fujikawa, K.; Tan, Y. H.; Nigudkar, S. S.; Stine, K. J.; Demchenko, A. V., Surface-Tethered Iterative Carbohydrate Synthesis: A Spacer Study. *The Journal of organic chemistry* **2013,** *78* (14), 6849-6857.

65.   Zeis, R.; Lei, T.; Sieradzki, K.; Snyder, J.; Erlebacher, J., Catalytic Reduction of Oxygen and Hydrogen Peroxide by Nanoporous Gold. *Journal of Catalysis* **2008,** *253* (1), 132-138.

66.   Yin, H.; Zhou, C.; Xu, C.; Liu, P.; Xu, X.; Ding, Y., Aerobic Oxidation of D-Glucose on Support-Free Nanoporous Gold. *The Journal of Physical Chemistry C* **2008,** *112* (26), 9673-9678.

67.   Déronzier, T.; Morfin, F.; Lomello, M.; Rousset, J.-L., Catalysis on Nanoporous Gold–Silver Systems: Synergistic Effects toward Oxidation Reactions and Influence of the Surface Composition. *Journal of Catalysis* **2014,** *311*, 221-229.

68.   Hu, K.; Lan, D.; Li, X.; Zhang, S., Electrochemical DNA Biosensor Based on Nanoporous Gold Electrode and Multifunctional Encoded DNA− Au Bio Bar Codes. *Analytical chemistry* **2008,** *80* (23), 9124-9130.

69.   Guo, M.-m.; Zhou, C.-h.; Xia, Y.; Huang, W.; Li, Z., Ultrasensitive Nonenzymatic Sensing of Glucose on Ni (Oh) 2-Coated Nanoporous Gold Film with Two Pairs of Electron Mediators. *Electrochimica Acta* **2014,** *142*, 351-358.

70.   Xiao, X.; Li, H.; Pan, Y.; Si, P., Non-Enzymatic Glucose Sensors Based on Controllable Nanoporous Gold/Copper Oxide Nanohybrids. *Talanta* **2014,** *125*, 366-371.

71.   Yan, M.; Jin, T.; Ishikawa, Y.; Minato, T.; Fujita, T.; Chen, L.-Y.; Bao, M.; Asao, N.; Chen, M.-W.; Yamamoto, Y., Nanoporous Gold Catalyst for Highly Selective Semihydrogenation of Alkynes: Remarkable Effect of Amine Additives. *Journal of the American Chemical Society* **2012,** *134* (42), 17536-17542.

72.   Qiu, H.; Xu, C.; Huang, X.; Ding, Y.; Qu, Y.; Gao, P., Immobilization of Laccase on Nanoporous Gold: Comparative Studies on the Immobilization Strategies and the Particle Size Effects. *The Journal of Physical Chemistry C* **2009,** *113* (6), 2521-2525.

73.   Wu, C.; Liu, X.; Li, Y.; Du, X.; Wang, X.; Xu, P., Lipase-Nanoporous Gold Biocomposite Modified Electrode for Reliable Detection of Triglycerides. *Biosensors and Bioelectronics* **2014,** *53*, 26-30.

74.   Kurtulus, O.; Daggumati, P.; Seker, E., Molecular Release from Patterned Nanoporous Gold Thin Films. *Nanoscale* **2014,** *6* (12), 7062-7071.

75.   Schlesinger, M., Electroless Deposition of Nickel. *Modern electroplating* **2000,** *4*, 667-684.

76.   Porter, L. A.; Choi, H. C.; Ribbe, A. E.; Buriak, J. M., Controlled Electroless Deposition of Noble Metal Nanoparticle Films on Germanium Surfaces. *Nano letters* **2002,** *2* (10), 1067-1071.

77.   Okinaka, Y.; Sard, R., Electroless Plating Process. Google Patents: 1974.

78.	Okinaka, Y.; Kato, M., Electroless Deposition of Gold. *Modern Electroplating, Fifth Edition* **2010**, 483-498.

79.	Okinaka, Y., *Electroless Plating of Gold and Gold Alloys*. Cambridge Univ. Press: **1990**.

80.	Magagnin, L.; Maboudian, R.; Carraro, C., Gold Deposition by Galvanic Displacement on Semiconductor Surfaces: Effect of Substrate on Adhesion. *The Journal of Physical Chemistry B* **2002,** *106* (2), 401-407.

81.	Srikanth, C. K.; Jeevanandam, P., Comparison of Galvanic Displacement and Electroless Methods for Deposition of Gold Nanoparticles on Synthetic Calcite. *Bulletin of Materials Science* **2012,** *35* (6), 939-946.

82.	Stuart, M. C., The Development of a Gold-Based Activator for Autocatalytic Plating. *Gold Bulletin* **1979,** *12* (2), 58-61.

83.	Molenaar, A., Autocatalytic Deposition of Gold- Copper Alloys. *Journal of The Electrochemical Society* **1982,** *129* (9), 1917-1921.

84.	Iacovangelo, C.; Zarnoch, K., Substrate- Catalyzed Electroless Gold Plating. *Journal of the Electrochemical Society* **1991,** *138* (4), 983-988.

85.	Qiu, H.-J.; Peng, L.; Li, X.; Xu, H.; Wang, Y., Using Corrosion to Fabricate Various Nanoporous Metal Structures. *Corrosion Science* **2015,** *92*, 16-31.

86.	Polat, O.; Seker, E., Halide-Gated Molecular Release from Nanoporous Gold Thin Films. *The Journal of Physical Chemistry C* **2015,** *119* (44), 24812-24818.

87.	Polat, O.; Seker, E., Effect of Surface–Molecule Interactions on Molecular Loading Capacity of Nanoporous Gold Thin Films. *The Journal of Physical Chemistry C* **2016,** *120* (34), 19189-19194.